Renal MRI: from Nephron to NMR Signal

Octavia Bane, PhD[1,2]; Erdmann Seeliger, MD[3]; Eleanor Cox, PhD[4]; Julia Stabinska, PhD[5,6]; Eric Bechler, PhD[7]; Sara Lewis, MD[1]; LaTonya J. Hickson, MD[8]; Sue Francis, PhD[4]; Eric Sigmund, PhD[9]; Thoralf Niendorf, PhD[10]

[1]Department of Diagnostic, Molecular and Interventional Radiology, Icahn School of Medicine at Mount Sinai, New York, NY, USA

[2]BioMedical Engineering and Imaging Institute, Icahn School of Medicine at Mount Sinai, New York, NY, USA

[3]Institute of Translational Physiology, Charité – University Medicine Berlin, Berlin, Germany

[4]Sir Peter Mansfield Imaging Centre, School of Physics & Astronomy, University of Nottingham, Nottingham, UK

[5]F.M. Kirby Research Center for Functional Brain Imaging, Kennedy Krieger Institute, Baltimore, MD, USA

[6]Russell H. Morgan Department of Radiology and Radiological Science, Johns Hopkins University School of Medicine, Baltimore, MD, USA

[7]Department of Diagnostic and Interventional Radiology, Medical Faculty, Heinrich Heine University Düsseldorf, Düsseldorf, Germany

[8]Division of Nephrology and Hypertension, Mayo Clinic, Jacksonville, Florida, USA

[9]Bernard and Irene Schwartz Center for Biomedical Imaging Center for Advanced Imaging Innovation and Research (CAI2R), New York University Langone Health, New York, NY, USA

[10]Berlin Ultrahigh Field Facility (B.U.F.F.), Max Delbrück Center for Molecular Medicine in the Helmholtz Association, Berlin, Germany

Corresponding Author:
Octavia Bane, PhD
1 Gustave L. Levy Pl.
New York, NY 10029
octavia.bane@mountsinai.org
401-523-91112

Grant funding: This work was funded by the US NIH NIDDK grant R01DK129888 (S.L., O.B.), and US NIH NCI grant R01CA245671 (E.S.)

Running title: Renal MRI: from Nephron to NMR signal

Renal MRI: from Nephron to NMR signal

Running title: Renal MRI: from Nephron to NMR signal

Renal diseases pose a significant socio-economic burden on healthcare systems. The development of better diagnostics and prognostics is well-recognized as a key strategy to resolve these challenges. Central to these developments are MRI biomarkers due to their potential for monitoring of early pathophysiological changes, renal disease progression or treatment effects. The surge in renal MRI involves major cross-domain initiatives, large clinical studies, and educational programs. In parallel with these translational efforts, the need for greater (patho)physiological specificity remains, to enable engagement with clinical nephrologists and increase the associated health impact. The ISMRM 2022 Member Initiated Symposium (MIS) on renal MRI spotlighted this issue with the goal of inspiring more solutions from the ISMRM community. This work is a summary of the MIS presentations devoted to (1) educating imaging scientists and clinicians on renal (patho)physiology and demands from clinical nephrologists, (2) elucidating the connection of MRI parameters with renal physiology (3) presenting the current state of leading MR surrogates in assessing renal structure and functions as well as their next generation of innovation, and (4) describing the potential of these imaging markers for providing clinically meaningful renal characterization to guide or supplement clinical decision making. We hope to continue momentum of recent years and introduce new entrants to the development process, connecting (patho)physiology with (bio)physics, and conceiving new clinical applications. We envision this process to benefit from cross-disciplinary collaboration and analogous efforts in other body organs but also maximally leverage the unique opportunities of renal physiology.

Keywords: Kidney, renal pathophysiology, imaging, MRI

1. Introduction

Kidney health is the unacknowledged key player in longevity and quality of life in countries of all development stages. Chronic kidney disease (CKD), claiming more than 1 million lives annually, is a global killer hidden in plain sight and an underappreciated challenge to healthcare systems (1). Kidney disease often progresses unnoticed until late into the disease course. Laboratory measures such as estimated glomerular filtration rate (eGFR) and albuminuria are key indicators of kidney dysfunction. Kidney biopsy remains the 'gold standard' for diagnostic (and prognostic) purposes but interpretation relies upon small tissue samples representing global kidney disease and exposes patients to procedural risks. Clinical evaluation of kidney disease widely employs ultrasound and computed tomography (CT) imaging to assess obstructive pathology, kidney size, blood flow, tumors, cysts, and stone burden. However, there is an unmet need for the development of non-invasive biomarkers to assess renal pathophysiology including interstitial fibrosis, hypoperfusion and hypoxia, inflammation, macrophage infiltration, and microvascular disease. The development of better diagnostics and prognostics which also limit procedural risk for patients is well-recognized as a key strategy to resolve these challenges.

Importantly, advancements in renal MR technology (**Figure 1**) and procedures allow assessment of microstructure (diffusion weighted imaging, T_1 mapping, MR elastography, diffusion tensor imaging, diffusion kurtosis imaging), hemodynamics (arterial spin labeling, intravoxel-incoherent motion, phase contrast MR, dynamic contrast-enhanced MR), oxygenation (blood oxygen-level dependent, quantitative susceptibility mapping), function (dynamic contrast-enhanced MRI), morphology, and inflammation. Collectively, MRI biomarkers have the potential to monitor early pathophysiological changes, renal disease progression or treatment effects, ideally in the entire kidney volume. One important example is total kidney volume (TKV), a prognostic enrichment biomarker approved by the US Food and Drug Administration (FDA) and European Medicines Agency (EMA), which informs disease altering therapy therein offering hope to individuals with polycystic kidney disease (PKD) (2,3). Ongoing kidney MRI advances expand non-invasive tools that propel CKD progression prediction, differentiate between acute tubular necrosis and rejection-induced injury in the kidney transplant, measure markers that may eventually replace current measures of kidney function (i.e. nephron number and single nephron GFR), and assess response to therapeutic interventions (i.e. hypoperfusion and hypoxia modification)(4). Kidney fibrosis, the final common outcome for all chronic diseases, remains a challenge to noninvasively quantify through MR elastography and other modalities (5). However, therapeutic targeting of multiple pathogenic processes is likely necessary to alter kidney fibrogenesis. Chronic sterile inflammation is increasingly recognized as a major contributor to progressive injury in several kidney diseases (6). For example, MR technology that non-invasively quantifies kidney macrophage density could reduce costs associated with kidney biopsy and histologic analyses and allow for repeated assessment over time.

Thus, advances in MR imaging technology that quantify kidney macrophage abundance *in vivo* could greatly enhance clinical tools available to nephrologists.

The emergence and standardization of renal MRI biomarkers involves major cross-domain initiatives (renalMRI.org, ISMRM Renal MRI study group, US NIDDK, UK Renal Imaging Network (UKRIN)), large-scale clinical studies and educational activities. These international collaborations have synthesized the current technical knowledge in a series of consensus technical review articles (7-12) and protocol descriptions (13), providing sample MRI protocols and guidelines for investigators who desire to start their own studies using quantitative MRI techniques. In parallel with these translational efforts, the need for greater (patho-)physiological specificity remains to enable engagement with clinical nephrologists and increase the associated health impact.

The ISMRM 2022 Member Initiated Symposium (MIS) "Renal MRI: from Nephron to k-space" spotlighted these developments with the goal of inspiring more solutions from the ISMRM and imaging sciences communities. This review article is a summary of the MIS presentations devoted to highlighting (1) the utilization of MRI by clinicians and imaging experts, in addressing current needs and possibly supplying new biomarkers to clinical use, (2) the needs for biological validation of renal MR markers to clarify the link to biology and physiology, (3) the current form of renal MRI technologies as well as next level innovations and (4) the potential added value of renal MR in patient management as a supplement or alternative to current clinical standards. As it summarizes the symposium presentations, this article, like the presentations themselves, is not a systematic review of kidney MRI literature to-date, nor is it a "how-to" technical implementation guide to the MRI techniques presented. For practical MRI protocol details, the readers are invited to consult the technical review references (7-12).

2. Renal physiology and pathophysiology – a primer for MR scientists

The major tasks the kidneys fulfill can be deduced from the classical symptoms of renal failure. These include retention of metabolic 'waste' products such as urea, retention of sodium and water with the ensuing volume expansion and arterial hypertension, potassium retention resulting in hyperkaliemia, and retention of protons resulting in disturbed acid-base-balance.

The nephron – the kidney's functional unit for urine formation and for maintaining water and electrolyte balances – is comprised of the glomerulus, in which primary urine is produced by ultrafiltration of blood plasma, and the tubule, which reabsorbs the vast majority of filtered water and osmolytes, but also secretes some substances, to produce the final urine. Both processes rely on intricate interactions of the nephrons with the vasculature (14). In conjunction with the kidney's unique vascular architecture, these interactions shape the renal-specific relationships among perfusion, energy metabolism and oxygenation

(15,16). The particularities of renal hemodynamics and oxygenation are of paramount importance for the pathophysiology of kidney disorders (15,17-19).

Total renal blood flow (RBF) is greater than in virtually all other organs: the kidneys receive about 20% of the cardiac output under resting conditions (14). While the renal mechanisms of autoregulation largely prevent physiological changes in systemic arterial pressure from exerting effects on RBF and GFR, RBF and GFR are nevertheless quite variable: for instance, they increase following a protein-rich meal and decrease during heavy exercise (14,20). Renal vascular resistance is determined by active vasomotion and passive compression of intrarenal vessels. With regard to pathophysiology, vasoconstriction mediated by sympathetic nerves, epinephrine, and angiotensin II, plays a prominent role, e.g. during hypovolemic shock, as does lack of vasodilatory nitric oxide in diabetic kidney disease (DKD) (21-23). Passive compression of intrarenal vessels plays a pathophysiological role in what is called intrarenal “compartment syndrome”: as the renal capsule is relatively rigid, any increase in intrarenal pressure as occurs, e.g. due to obstruction of the urinary tract, tubular congestion, or occlusion of the renal vein, results in reduced perfusion and oxygenation (24-26). Both active vasomotion and passive compression of intrarenal vessels do not only alter blood flow but, at the same time, also the blood volume per tissue volume, i.e. the intrarenal blood volume fraction. This is of high relevance for physiological interpretation of MR-based assessments of renal oxygenation by blood oxygenation level-dependent (BOLD) techniques, as will be detailed in section **3b**. The MRI relaxation times T_2* and T_2 provide surrogate markers of tissue oxygenation. However, T_2*, T_2 reflect the amount of deoxygenated hemoglobin (deoxyHb) per tissue volume, therefore the relationship of renal T_2*,T_2 with tissue oxygenation is also dependent on (changes in) the blood volume fraction (27-30).

GFR depends on the total filtration area of all glomeruli, their hydraulic conductance, and on the balance of four pressures. Typical examples for reductions of the filtration area are nephrectomy and the gradual loss of functional nephrons with age and in CKD. Following nephrectomy this is partially compensated for by hyperfiltration by the remaining kidney. Hyperfiltration of the (remaining) functional nephrons occurs also in the initial stages of CKD and in early DKD (15,23,31). The blood pressure in the glomerular capillaries drives glomerular filtration, whereas plasma oncotic pressure and fluid pressure of the primary urine in Bowman’s capsule hinder it. A fourth pressure comes into play in pathophysiological conditions only, namely, when sizable amounts of plasma proteins are filtered, which increases oncotic pressure in Bowman’s capsule. The balance of the four pressures – termed effective filtration pressure – determines present GFR (14). Each of the pressures may vary under (patho-)physiological conditions. Glomerular capillary pressure varies with both active vasomotion and passive vascular compression, whereby increased preglomerular vascular resistance decreases GFR while increased postglomerular

resistance increases it (14). Plasma oncotic pressure increases, e.g. in dehydration, and decreases, e.g. in nephrotic syndrome. Increase in fluid pressure in Bowman's capsule as occurs due to obstruction of the urinary tract or tubular congestion reduces GFR (14,18,32).

In healthy adults, GFR amounts to about 180 liters per day. This is about fourfold the amount of total body water of an average adult (14)! In order to maintain body water content, water balance must be achieved, i.e. renal water excretion must exactly match water intake minus extrarenal water loss, both of which are quite variable. On average about 99% of the filtered water must be reabsorbed by the tubules. The daily amount of sodium filtered in the glomeruli is the equivalent of about 1500 grams of table salt (14). Again, in order to maintain body sodium content, renal excretion must exactly match sodium intake minus extrarenal loss, both of which vary considerably (33). Considering that our daily average salt intake nowadays amounts to 10 grams, it becomes clear that at least 99% of the about 1500 grams of filtered sodium must be reabsorbed by the tubules. All tubular reabsorption ultimately relies on energy-depending processes: sodium reabsorption requires about 90% of the renal energy expenditure and, thus, of oxygen (O_2) consumption (15,16). In contradistinction to virtually all other organs, where O_2 consumption determines perfusion, it is the other way around in the kidney: the higher the GFR the more sodium must be reabsorbed by the tubules. As GFR, in general, varies with RBF, renal perfusion determines renal oxygenation (15,16).

In accordance with the huge total RBF, the whole kidneys' O_2 extraction is much lower than in all other organs. Yet, blood perfusion within the kidneys is quite heterogeneous: while 100% of total RBF reaches the cortex, only 15% of blood that previously passes through the cortex, reaches the medulla. Medullary perfusion relies on capillaries and vasa recta only, as there are no arteries or arterioles supplying it. This unequal distribution is one reason behind the very low tissue partial pressure of O_2 (pO_2) in the medulla (15,16,28). The other reason is O_2 shunt diffusion from arteries to veins in the cortex and from descending to ascending vasa recta in the medulla (16,28).

These specifics of renal hemodynamics and oxygenation may explain why the kidneys are quite vulnerable to injury and disorders. Acute kidney injury (AKI) is triggered by a variety of causes, yet, irrespective of the etiology, there is a common early element in AKI pathophysiology: renal tissue hypoperfusion and hypoxia. Imbalance between renal O_2 delivery and demand also promotes progression from AKI to CKD. It furthermore plays a prominent pathophysiological role in DKD (15,17-19). Finally, the development of renal fibrosis – be it triggered by inflammatory responses to AKI and its progression to CKD, by DKD, autoimmune diseases, or hereditary diseases such as PKD – in general, leads to rarefication of intrarenal vessels and, thereby, to a vicious cycle of ever increasing renal O_2 deficits. In other words, the imbalance in the O_2 delivery/demand becomes self-perpetuating (5,19,34,35).

As the fibrosis-induced rarefication of intrarenal vessels decreases the blood volume fraction and, thereby the amount of deoxyHb per tissue volume, this impact on T_2*, T_2 must be taken into account when interpreting renal BOLD-MRI.

2.a. Diagnosis: Current biomarkers and the role of MRI

Current options for effective prophylactic and therapeutic regimen for the majority of kidney disorders are disappointingly sparse. One generally recognized major obstacle is the notorious lack of clinically available diagnostic tools that would allow early recognition of patients undergoing AKI, and recognition of CKD with sufficient sensitivity and specificity. In accordance with current clinical practice guidelines, AKI and CKD are still diagnosed, and their staging determined, based largely upon measurements of the serum concentration of creatinine (SCrea), a surrogate marker for GFR. To overcome the well-known limitations of SCrea-based metrics including estimated GFR (eGFR), several alternative blood- or urine-based markers reflecting renal injury, inflammation, fibrosis, or repair have been proposed. Despite promise, the clinical performance of these markers has been modest, and none has advanced to provide point-of-care diagnosis. In general, these markers fail to reveal early events in AKI pathophysiology, such as tissue hypoxia (18,36,37). Recognizing these limitations, synergistic approaches that include MRI are warranted (38-42).

2.b.Histopathological diagnosis of kidney disease

Renal biopsy is the clinical “gold standard” for qualitative evaluation of kidney tissue. Despite its invasiveness, biopsy provides access to tissue for research purposes, such as advanced histopathology, immunohistochemistry, proteomics and metabolomics quantification. Research collaborations such as the Kidney Precision Medicine Project (KPMP) at the U.S. NIDDK conduct prospective kidney biopsies in acute and chronic disease for deep molecular (and imaging) phenotyping (43).

Kidney core needle biopsy is used since the 1950s, and is performed with automated devices under ultrasound guidance since the 1980s (43). Common indications include unexplained proteinuria, hematuria, rapid kidney function loss, or to monitor response to treatment. Kidney allograft biopsies are often performed as an initial post-implantation biopsy to assess the health of the allograft and thereafter “for cause” to assess dysfunction. A minority of transplant centers perform “protocol” biopsies at fixed intervals, particularly in patients at higher risk for rejection. A good quality biopsy specimen will generally contain 2 tissue cores of 1-2 cm in length, with mostly cortical (vs. medullary) tissue, and 10-15 visible glomeruli (43). To minimize the procedural risk, sample collection is usually limited to 2-3 but fewer than 5 needle passes despite adequacy of sample (43).

Stains are performed for cell nuclei (H&E), glomerular basement membranes (period acid-Schiff), collagen, fibrous tissue (hematoxylin phloxine saffron, Sirius red, Congo red, Masson’s trichrome), in

addition to immunofluorescence studies used to identify glomerular diseases, according to each institution's protocols. A renal pathologist scores the presence of fibrosis, inflammation, vascular and glomerular disorder qualitatively, on a scale of 0-3 according to increments of 10%, then 25% of tissue that show pathological changes (43). Kidney transplant biopsies are scored according to the Banff system (44), a complex scoring system with 15 scores classifying interstitial fibrosis, vascular, tubular and interstitial inflammation, as well as glomerular and vascular disease.

Less than 0.0001% of the renal tissue is sampled in a core needle biopsy. A report of 310 biopsies from 155 patients concluded that chronic allograft injury was misclassified in 25% of biopsy specimens (45). Histopathological lesions, especially interstitial fibrosis/tubular atrophy (IFTA), are patchy and heterogeneously distributed throughout the kidney allograft (45). Biopsy, particularly in allograft injury, is thus prone to profound sampling error and high inter/intra-observer variability (46,47). In terms of biopsy risks and complications, recent meta-analyses show that while risk of major complications (0.3% of patients with bleeding requiring intervention in native and transplant biopsy), or death is infinitesimal (1 in 1,667 patients with native and 5 in 38,593 with transplanted kidneys), there are non-negligible risks (perinephric hematoma in 11% of native and 1.63% of transplanted kidneys, macroscopic hematuria in 3.5% of native and 3.2% of transplant biopsy (48-50)).

Taken together, while traditional biopsy methods offer the advantage of direct evaluation of renal tissue, disadvantages are sampling bias, qualitative and subjective clinical interpretation, and a non-negligible rate of complications.

MRI facilitates non-invasive assessment of several structural and functional kidney features (**Figure 1**). As detailed below, several MRI tools provide physiologic specificity. A growing literature shows its potential to inform on the different stages of renal pathophysiology, improve prediction and interception of disease progression and evaluate treatment of renal disease.

3. Renal structural and functional MRI: what are we measuring, what is its added clinical value?

3.a MRI-based assessment of kidney size

Since changes in kidney size (KS) are associated with several renal pathologies, an increasing body of literature assesses the potential of non-invasive imaging-derived KS as a clinical parameter for diagnosis, prognosis, and treatment evaluation (41,51,52). In patients suffering from PKD, KS correlates with disease progression and GFR (53). Consequently, KS has been approved as a prognostic marker for clinical trials of therapies for autosomal dominant PKD (2,3). Detecting KS reduction due to parenchymal atrophy, sclerosis, and fibrosis has been demonstrated to identify CKD and to determine its severity (51). Longitudinal MR-based KS monitoring is proposed as a key measure for several kidney disorders including hyperfiltration in early DKD, renal transplants, renal artery stenosis, and vesicoureteral reflux

(41). If performed manually, segmentation of the kidneys is time consuming, and dependent on the experience and skill of the image analyst. Methods using deep learning convolution neural network (CNN) U-Net models are now becoming available for automated segmentation of KS to assess TKV in health and disease, as well as cortex and medulla segmentation. These models must be trained and tested on a given image contrast and slice orientation using accurate manual segmentations to achieve good accuracy. A number of studies have shown improvements for estimation of KS in PKD using T_1- and/or T_2-weighted imaging (54,55), including a study using MRI scans from the National Institute of Diabetes and Digestive and Kidney Disease (NIDDK) Consortium for Radiologic Imaging Studies of Polycystic Kidney Disease (CRISP) study (56). Recent studies have demonstrated the use of whole-body T_1-weighted dual echo gradient echo (GRE) sequences to estimate KS in in the UK Biobank (UKBB) (57) and German National cohort (NAKO) large scale population studies(58). Segmentation of TKV, and separation of the cortex and medulla is more challenging in Chronic Kidney Disease due to both the reduction in KS and reduction in cortical-medullary differentiation. Automated segmentation of T_2-weighted MR images using a CNN in healthy controls and CKD patients has been shown to be robust to accurately segment to calculate TKV (59). Most recently, a CNN has been shown to be able to automatically segment the renal cortex and medulla from MOLLI T_1 maps in transplanted CKD patients (60).

That KS changes are indicative of pathophysiologic developments has been demonstrated by serial MRI in a variety of models. These include models that emulate clinical conditions such as i) ureteral obstructions due to urolithiasis or during upper urinary tract endourologic procedures, ii) administration of X-ray contrast media (CM) for cardiac procedures, iii) obstructions of the renal vein during partial nephrectomy or due to renal cell carcinoma-derived thrombus formation, and iv) clamping of the suprarenal aorta or renal artery during surgery or the low arterial target pressure during cardiopulmonary bypass (25). MR-based KS assessment was also used in experimental diabetes, mutant models mimicking PKD, and renal allografts (61-63). A recent preclinical study demonstrated that monitoring KS allows for physiological interpretation of MRI-based oxygenation changes in acute pathophysiologically relevant scenarios (26).

3.b. MRI-based assessment of renal oxygenation

Pre-clinical studies

Given the pivotal and early prognostic pathophysiological role of renal tissue hypoxia, MRI-based assessment of renal oxygenation by blood oxygenation level-dependent (BOLD) techniques could become a vital assay for research into renal (patho-)physiology and for clinical application This approach is based on the magnetic susceptibility of blood, with deoxygenated hemoglobin (deoxyHb) being

paramagnetic and oxygenated hemoglobin being diamagnetic. Increases in the concentration of deoxyHb induces reductions in the MRI relaxation times T_2^* (=1/R_2^*) and T_2 (=1/R_2). T_2^*, T_2 provide surrogate markers of tissue oxygenation due to their dependence on the O_2 saturation of hemoglobin (StO_2) and its relationship to the pO_2 in blood and tissue (27,40). However, T_2^*,T_2 reflect the amount of deoxyHb per tissue volume, therefore the relationship of renal T_2^*,T_2 with tissue pO_2 is also dependent on the blood and tubular volume fractions (27-29,40). While an ever-increasing number of experimental and clinical studies utilize renal BOLD-MRI, it cannot yet be regarded as a quantitative biomarker. Such a designation requires standardization of MRI protocols for both preclinical and clinical studies as well as calibration against 'gold standard' quantitative methods (7,27,64). The 'gold standard' probes for the pathophysiologically relevant parameter tissue pO_2 are invasive, thus, calibration can only be done in preclinical studies (16,65). For this purpose, a multimodality setup (MR-PHYSIOL) was developed that combines invasive measurements including tissue pO_2 with parametric MRI, allowing simultaneous *in vivo* measurements in the same rat kidney. Dedicated acute (patho-)physiologically relevant test interventions performed by remote control proved instrumental to detail the link between renal tissue pO_2 and T_2^*, T_2 including the role of the confounding factors vascular and tubular volume fraction in these scenarios (40,65,66) .

Human studies on renal oxygenation necessitate non-invasive approaches, preferable, in a stand-alone MRI setting. Recognizing that events leading to acute renal hypoxia are often associated with changes in the blood and/or tubular volume fractions, and that these changes are mirrored by changes in kidney size, dynamic MRI to monitor KS in parallel with T_2^*,T_2 was recently shown to enable physiological interpretation of acute T_2^*,T_2 changes (26). In this preclinical study, serial *in vivo* mapping of T_2^*,T_2 was performed during clinically realistic interventions which alter renal tissue oxygenation reversibly – including a brief occlusion of the suprarenal aorta (OA), the renal vein (OV), or both (OAV) – and with longer-lasting effects – including injection of an X-ray CM. As shown by **Figure 2**, OA resulted in a decrease in KS and a moderate decrease in T_2^*,T_2, OV resulted in an increase in KS and a much more pronounced decrease in T_2^*,T_2, and OAV left KS unchanged and resulted in an intermediate decrease in T_2^*,T_2. Previous studies with 'gold standard' probes showed an equivalent decrease in tissue pO_2 upon the three occlusions (66). The reason for this discrepancy is that changes in T_2^*,T_2 reflect changes in the amount of deoxyHb per tissue volume rather than directly mirroring StO_2. In addition to decreased StO_2, intrarenal blood volume is reduced upon OA, increased upon OV, and unchanged upon OAV. Thus, correct interpretation of T_2^*,T_2 as surrogate markers for acute changes in renal tissue oxygenation must take into account changes in KS. If T_2^*,T_2 decrease and KS remains unchanged, tissue oxygenation is reduced. If T_2^*,T_2 decrease and KS also decreases, the pO_2 reduction is more severe than if KS is unchanged; if T_2^*,T_2 decrease and KS increases, the pO_2 reduction is less severe.

Administration of an X-ray CM induced a sustained KS increase, with an initial increase in T_2*,T_2 followed by a moderate decrease (26). Measurements by 'gold standard' probes showed an immediate, massive and sustained drop in pO_2 (67). The explanation for this apparent discrepancy becomes clear from the observed KS increase, which reflects the 'compartment syndrome' that results in compression of the intrarenal vessels and thus in decreased deoxyHb. This result underscores how MRI-based measurement of renal oxygenation by T_2*,T_2 is crucially dependent on monitoring accompanying changes in KS. Taken together, this study demonstrated that monitoring KS allows physiological interpretation of acute renal oxygenation changes obtained by T_2*,T_2 (26).

Human studies

Given the pathophysiological role of renal tissue hypoxia for CKD progression, BOLD-MRI has been used in patients with CKD to assess its diagnostic potential. These studies have produced inconsistent results (68-72). Apart from different MRI acquisition and analysis protocols, major potential reasons for these inconsistencies include CKD-related reductions in the intrarenal blood volume fraction due to rarefication of vessels in fibrosis or reduced vascular lumen due to vascular remodeling, e.g. in kidney disease associated with hypertension. These alterations will greatly vary according to the disease etiology and stage. Moreover, in most CKD studies, the main clinical marker renal BOLD was benchmarked against, was notoriously insensitive SCrea/eGFR (73). However, in a prognostic study, Pruijm et al. measured BOLD-MRI in 112 patients with CKD, 47 with hypertension but without CKD and 24 healthy controls, and all participants underwent a physical examination, blood and urine sampling as well as an ultrasound scan (74). Pruijm et al. observed that CKD patients with increased $R_2^*=1/T_2$* (low oxygenation) in the cortical layers and a flat corticomedullary R_2^* slope had a faster yearly decline in eGFR and were ten times more likely to develop an adverse renal outcome. Therefore, R_2^*-based assessment of renal tissue oxygenation might be used as a predictor of GFR decline in CKD.

Another area of application is in kidney transplantation, wherein discovery of non-invasive diagnostic measures to assess kidney allograft dysfunction is needed. Han et al. (75) tested whether acute rejection (AR) and acute tubular necrosis (ATN) could be differentiated by BOLD-MRI. They measured 110 patients, with 28 patients having a biopsy-proven AR (n = 21) and ATN (n = 7). AR kidney allografts showed significantly lower medullary R_2^* values (higher oxygenation), while ATN allografts revealed higher R_2^* in the cortex. Additional investigations applying BOLD-MRI in kidney transplants also identified a loss of corticomedullary R_2^* differentiation in allografts with acute dysfunction (76). Finally, BOLD-MRI has been successfully used to assess response to novel therapeutics. In an early phase clinical trial in patients with atherosclerotic renovascular disease, intraarterial renal infusion of

mesenchymal stem cells improved renal blood flow and fractional hypoxia (expressed as % R_2^* >$30s^{-1}$) decreased in the stenotic kidney (77).

BOLD-MRI has very well-recognized limitations. Changes in T_2* are not only caused by differences in renal blood oxygenation but also by other physiological parameters such as renal blood volume fraction (28,78,79). Therefore, the question was raised whether the interpretation of BOLD-MRI as a surrogate for renal tissue oxygenation is universal (30). Second, the BOLD-signal is not only influenced by the paramagnetic deoxyHb, but also by other underlying tissue susceptibilities like diamagnetic proteins (80). Additionally, scanner related factors such as eddy currents or magnetic field inhomogeneity also affect T_2^*. This makes it difficult to compare BOLD data across multiple sites (81).

Renal quantitative susceptibility mapping (QSM)

To overcome the constraints of BOLD-MRI, QSM facilitates direct probing and quantification of the underlying magnetic susceptibility of tissue while removing scanner related factors (82). QSM utilizes the phase information of the image data to determine magnetic susceptibility maps of the tissue. QSM provides a high structural contrast that is sensitive to changes in tissue microstructure and chemical composition (83). However, QSM requires complex, non-trivial post-processing, including solving ill-posed inverse problems (84-86). In essence, the information needed for QSM is encoded in any susceptibility sensitized BOLD protocol that uses a range of susceptibility weighting. This has the advantage that BOLD-MRI and QSM can be performed with a single measurement and without additional scan time.

There is a limited number of studies on abdominal QSM due to challenges including respiratory movement, substantial changes in susceptibility at tissue interfaces and the presence of subcutaneous and visceral fat. An early study used QSM to detect inflammation and fibrosis in ex-vivo mice kidneys (87). All mice kidneys with inflammation and fibrosis exhibited a more diamagnetic susceptibility in the cortex, outer and inner medulla when compared to healthy controls. This decrease in susceptibility accompanies the increase of diamagnetic lipids and proteins associated with inflammation and fibrosis (88).The literature shows very few examples on in-vivo renal QSM in the humans (80). One demonstrates for a single patient that fibrotic kidney displayed the same decrease in susceptibility as the above-mentioned mice study (**Figure 3**). Broader clinical studies are warranted to evaluate the potential role of QSM as a diagnostic marker for kidney pathologies.

3.c. Renal blood flow and perfusion

Blood flow into the kidney can be assessed by measuring the bulk flow within the renal artery using phase contrast (PC)-MRI. Renal tissue perfusion can be measured with dynamic contrast enhanced (DCE)-MRI or arterial spin labelling (ASL)-MRI.

Phase contrast MRI (PC-MRI)

PC-MRI uses velocity-encoding (V_{ENC}) magnetic field gradients to generate phase shifts proportional to the velocity of protons in the direction of the gradient. Flow measurements are most accurate when the imaging plane is perpendicular (through-plane) to the vessel of interest (**Figure 4A**). The V_{ENC} must be higher than the peak velocity to avoid phase aliasing, typically 100-120cm/s to measure renal artery blood flow. PC-MRI data are typically collected in a breath hold with the use of retrospective or prospective cardiac gating to synchronize data acquisition with the cardiac cycle. For PC-MRI analysis, a region of interest (ROI) is placed in the renal artery. To obtain the arterial flux (in ml/min) at each cardiac phase, the velocity (in cm/s) can be multiplied by the area (in mm^2) in each frame (**Figure 4B**). Global perfusion of the kidney (in ml/min/100 ml tissue) is obtained from the ratio of mean arterial flux by total kidney volume (ml) multiplied by 100.

Careful consideration is required for acquisition, quantification and reporting of PC-MRI (8,89). A good vascular survey is required, such as a time-of-flight (TOF), or inflow enhancement scan to position the imaging plane perpendicular to the renal artery and close to the aorta prior to any bifurcations (**Fig 4A(ii)**). The spatial resolution must be sufficient to include several voxels from within the vessel, whilst keeping the breath hold short and retaining sufficient signal-to-noise ratio (SNR). Parallel imaging can be used to reduce scan time or to increase the spatial resolution. Images affected by severe movement should be discarded, and if aliasing occurs data can be phase unwrapped. The between session coefficient of variation (CoV) of renal artery blood flow measured using PC-MRI ranges from 8 to 23% (89).

4D flow PC-MRI uses blood flow encoding in 3 directions. This removes the need for detailed planning and allows several vessels to be assessed simultaneously (90,91). Further work should focus on calibration of PC-MRI using flow phantoms, standardization and availability of analysis software including motion correction, and the comparison of semi-automatic and manual ROI selection.

Dynamic contrast enhanced MRI (DCE-MRI)

DCE-MRI uses an exogenous contrast agent, typically gadolinium-based, which is filtered in the glomeruli. A rapid series of T_1-weighted images is collected, before and during the passage of a contrast agent bolus. The signal-time-curve (STC) reflects the passage of the contrast through the kidney tissue

(92). Analysis of DCE-MRI data comprises kidney segmentation, delineation of the arterial input function (AIF) from the aorta, calculation of T_1 maps to convert voxel-wise STCs to concentration time curves, before model-based quantification of renal perfusion (in ml/100ml/min) and glomerular filtration rate (in ml/min). Good SNR and high temporal resolution are required to define the AIF.

A study by de Boer et al.(93) measured DCE as part of a multiparametric repeatability study in healthy subjects and showed a correlation between visits. However, Bland-Altman limits of agreement were large (186 to -202 ml/100ml/min). Eikefjord et al.(94) performed a reproducibility study of healthy volunteers where a correlation was seen between scanning sessions, but the intraclass correlation coefficient (ICC) was low (0.34). DCE is widely used in animal research, but its clinical utility is limited by the risk of nephrogenic systemic fibrosis in patients with low GFR. Another limitation of renal DCE-MRI that hampers its clinical adoption is the complex post-processing pipeline, and the lack of consensus regarding the best pharmacokinetic model for fitting the data, even for the same contrast agent.

Arterial spin labeling (ASL)

ASL uses endogenous arterial blood water to measure renal perfusion, and is consequently safe for patients with renal impairment. Images with and without labeling of inflowing arterial blood are acquired, with the difference providing a perfusion-weighted image. Renal perfusion is quantified in units of ml/100g/min with appropriate modeling.

The two labeling schemes recommended for renal ASL (10) are pseudo-continuous ASL (PCASL) and the pulsed ASL (PASL) Flow-sensitive Alternating Inversion Recovery (FAIR) scheme. In FAIR ASL, a non-selective adiabatic inversion slab centered at the imaging plane is applied to label inflowing arterial blood while for the control acquisition a selective inversion slab inverts the magnetization in the imaging plane only (**Figure 5A**). The inversion time should be chosen to allow the labeled blood to arrive and exchange with the renal tissue. In PCASL, the blood is inverted as it flows through the labeling plane, which is positioned over the aorta (**Figure 5B**).

ASL has intrinsically low SNR, therefore multiple repetitions are averaged. Short echo times increase SNR and reduce the impact of respiratory motion. Fast acquisitions allow optimal sampling of the highest ASL difference signal. Spin echo-echo planar imaging (SE-EPI) provides the highest temporal SNR and lowest variability in perfusion (95). Respiratory motion challenges ASL-MRI because it exceeds clinically acceptable breath-hold times. Free breathing with coaching, guided breathing or respiratory triggering are better suited. Background suppression (BGS) of static tissue is often used to improve ASL sensitivity, but this can affect the success of image realignment (96-98).

A simple perfusion model neglects tissue transit delays and MRI signal relaxation differences between blood and tissue, which results in underestimation of perfusion. Alternatively, data can be collected at multiple inversion times to determine tissue transit delays, however this approach is time consuming. A faster solution is to acquire a series of images following each inversion pulse (99) for iterative perfusion modelling (100). Renal cortical perfusion measured by ASL ranges from 200 to 350 ml/100g/min (101). The between-visit CoV of renal cortical perfusion is ~10% (102) but increases up to 20% when BGS is used (96). Reproducibility of FAIR and PCASL between two sessions showed CoV of 10% for FAIR and 34% for PCASL (97).

A review (103) compared DCE with ASL, with some studies reporting higher perfusion values from DCE than ASL, whilst others showed no difference. DCE has a larger CoV than ASL (27-32 vs. 14-18% (104), 17 vs. 10% (93)) with larger confidence limits for DCE compared with ASL (186 to -202 vs. 110 to -91 ml/100g/min(93)). Alhummiany et al. found no differences between PC-MRI, DCE and ASL in a cohort of type-2 diabetes patients (105). Bland-Altman and correlations between each of the measures showed PC-MRI and ASL to have the best agreement. The repeatability error is lower for PC-MRI than for ASL in healthy volunteers (79 ± 41 vs. 241 ± 85 ml/min/1.73m^2).

Several reports highlighted that eGFR positively correlates with perfusion measured by ASL (95,106-109) and PC-MRI (95). Renal perfusion reduces with age, as shown using ASL (110,111), DCE (112), and PC-MRI (101). Renal perfusion is reduced in CKD (51,110,113,114) and at peak AKI (115). In these AKI patients, eGFR was normal after one year, but some participants still had lower than expected renal perfusion, potentially indicative of patients at risk of further AKI episodes or progression to CKD. The diagnostic potential of ASL to diagnose AKI was investigated (116). However, the correlation of SCrea with renal perfusion in healthy volunteers was lost in the patient group. PC-MRI blood flow was reduced in septic AKI compared with healthy volunteers (117). ASL perfusion and PC-MRI renal blood flow are reduced during AKI in COVID-19 (118).

3.d. Renal microstructure and microcirculation

Basic concepts of diffusion-weighted imaging: water motion and microstructure

MRI signal arising from water protons *in vivo* is sensitive to tissue composition and structure in a complex manner, both through longitudinal and transverse relaxation processes as well as through molecular motion and diffusion effects. These thermally or physiologically driven random movements of water molecules can be probed on a microscopic scale using diffusion-weighted imaging (DWI; **Figure 6A**), providing unique information on the functional architecture of tissues. In biological tissues, molecular water motion is restricted by many obstacles including cell membranes, interstitial matrix and directional

structures such as the renal tubules and blood vessels in the kidney. As a result, the observed diffusion coefficient (a measure of mean-square displacement per unit time) in an imaging voxel containing a mix of all these different diffusion environments is called the apparent diffusion coefficient (ADC). As tissue microstructure is considered the major determinant of apparent diffusion, changes in cellular density, water content, cell membrane integrity, structural organization, and the presence of macromolecules can cause alterations in ADC and motivate the use of DWI for diagnosis and monitoring of kidney pathologies.

ADC maps are derived from the voxel-wise fitting of the DWI signal acquired at different b-values (with different levels of diffusion weighting) to a mono-exponential model (**Figure 6B, C and D**). ADC represents the most widely used diffusion biomarker and its potential clinical value has been demonstrated in patients with CKD (119), kidney allograft dysfunctions (120,121), acute pyelonephritis (122,123), PKD (124), obstruction of the urinary tract (125), and renal artery stenosis (126). With the exception of PKD, all of the studies reported lower parenchymal ADCs in patients than in healthy controls. Moreover, ADC displayed a good correlation with the histopathologic degree of renal fibrosis (119,127), and SCrea/eGFR (128,129). Although ADC is a promising imaging marker, it should be noted that renal DWI signal is not truly mono-exponential and ADC is a purely empirical parameter representing a mix of all potential contributors to the diffusion NMR signal. This multifactorial dependence of ADC complicates the interpretation of the observed signal changes that can reflect impaired renal function and reduced perfusion and/or the degree of renal fibrosis, and/or other histologic features. This ambiguity motivates development and application of more advanced acquisition protocols and DWI signal modeling approaches.

Renal microcirculation and tubular flow: intravoxel incoherent motion (IVIM)

Urine formation by glomerular filtration and tubular water reabsorption involve considerable microscopic flow in blood vessels and tubules. Consequently, the contribution of the flow-driven pseudo-diffusion component to the measured DWI signal in the kidney is substantial. The effects of blood flow in the renal microvasculature and 'true' tissue diffusion can be separated and quantified using an intravoxel incoherent motion (IVIM) model (130), which improves the interpretation of the diffusion-attenuated MR signal versus a mono-exponential ADC model (131). IVIM imaging has been applied in CKD patients (132), renal artery stenosis (133), urinary tract infections (134), and kidney allograft dysfunctions (135). The original two-compartment IVIM model assumes that the incoherent blood flow in the microvasculature results in a fast-decaying signal component with pseudo-diffusion coefficient D_{fast} (or D_p, D*) and signal fraction f_{fast} (or f_p, f), whereas the water molecules motion in the renal tissue contributes to the slow water diffusion component described by a diffusion coefficient D_{slow} (or D_t, D). More recently, it has been recognized that the intra-tubular fluid compartment contributes to the pseudodiffusion term

as well, and its contribution can be modeled by a third intermediate component characterized by D_{inter} (or D_i) and f_{inter} (or f_i) in the renal DWI signal (136,137) **(Figure 6E).**

While multi-compartment IVIM models are more suitable for the representation of diffusion properties of the kidney, the literature shows a rather large variability in reported IVIM parameter values. This divergence is mainly related to the diversity of acquisition and post-processing protocols, which ask for harmonization and standardization (9,138). In multi-platform studies, gradient non-linearity (in which the ratio of actual to nominal b-values varies with the square of the gradient amplitude, away from isocenter), shim and eddy currents introduce bias in fitted parameter values. Of these sources of bias, gradient non-linearity is the most important in off-isocenter organs such as the kidneys and can be assessed by an ice-water diffusion phantom and corrected by site or vendor-derived correction factors (139). Furthermore, renal DWI is sensitive to cardiac activity and blood pulsation (140,141) and to diuretic challenges (142).

Renal microstructure: diffusion tensor imaging (DTI)

Besides providing functional information on renal microcirculation and tubular flow, DWI can be used to probe diffusion directionality as an indicator of functional loss and structural damage in different renal pathologies. One of the most unique features of DWI is its sensitivity to water motion only along the direction of the magnetic field gradient. Consequently, it is possible to probe anisotropic microstructure by measuring preferential water diffusion directions. Diffusion tensor imaging (DTI) is particularly suitable for studying kidney microstructure including tubular structures and blood vessels that contribute to spatially restricted diffusion of water molecules. Overall, the radial orientation of tubular structures and vessels in the renal medulla results in more restricted water diffusion compared to cortex which contains more randomly oriented structures. Fractional anisotropy (FA; **Figure 6F**) and axial diffusivity (AD), which represent the degree of diffusion anisotropy and the rate of diffusion along the preferential diffusion direction, are higher in the medulla than the cortex. Conversely, mean diffusivity (MD) and radial diffusivity (RD), which describe the average mobility of water molecules and diffusivity perpendicular to the principal diffusion direction, show higher values in the cortex compared to medulla.

DTI supports the study of renal microstructure in healthy human subjects and patients with various kidney pathologies including CKD (143-145), DKD (146), glomerulonephritis (147), kidney transplant dysfunction (135,148,149) and PKD (150,151). Most of these studies reported lower medullary FA in diseased kidneys compared to the healthy ones, indicating a reduction in diffusion anisotropy due to pathological changes in the renal parenchyma, such as interstitial fibrosis and/or tubular atrophy. These findings suggest that FA may be a useful imaging marker of structural alterations regardless of the etiology of the underlying disease. Moreover, the results obtained in PKD patients and renal allograft

recipients show that besides FA also the length, number and density of the DTI tracts can be used to evaluate renal microstructural damage quantitatively and visually.

Diffusion kurtosis imaging (DKI)

Conventional DWI assumes that diffusion-driven water displacement can be described by a Gaussian distribution. In reality, complex cellular microstructure greatly affects the random motion of water molecules and, consequently, their distribution deviates considerably from the normative pattern. This non-Gaussian diffusion behavior can be probed by means of diffusion kurtosis imaging (DKI), which extends conventional DWI by quantifying the degree to which the water diffusion probability distribution function varies from the normal distribution. DKI provides a dimensionless measure of the diffusion hindrance and restriction known as kurtosis, which can be considered as a reflective marker of tissue heterogeneity that vanishes for Gaussian diffusion. Qualitatively, higher kurtosis values suggest more impediments to normal diffusion and thus greater microstructural complexity. The potential diagnostic value DKI was investigated in patients with hyperuricemia (152), immunoglobulin-A-nephropathy (153) and CKD (154). Overall, higher renal parenchymal mean kurtosis (MK) were found in subjects affected by asymptomatic hyperuricemic injury and gouty arthritis than in controls (152). A similar trend was observed in CKD patients. A positive correlation between MK and glomerular injury and tubulointerstitial lesion, and a negative correlation between MK and eGFR were reported (154). These studies indicate that cortical MK values have higher sensitivity to renal pathology and function associated with CKD progression than ADC.

Advanced variants of renal DWI

Although DTI and IVIM can separately quantify microstructural anisotropy and microcirculation in the kidney, it is known that each of these representations provides only a partial description of the measured renal DWI signal. In particular, it has been shown that both tubular/vascular flow and tissue diffusion contribute to the medullary anisotropy (155). Therefore, there is a growing interest in developing more advanced DWI variants that more accurately describe the diffusion properties of the kidney. Among these, approaches such as a generalized intravoxel oriented flow (IVOF) (156,157) model and Renal Flow and Microstructure AnisotroPy (REFMAP) (141,155,158) use a hybrid IVIM/DTI methodology to simultaneously measure renal diffusion anisotropy and flow effects, accounting not only for diffusion anisotropy but also for the anisotropy of the flow compartment.

Recent developments resolved contributions from tubular and vascular compartments based on the differences in pseudo-diffusion rate using data-driven non-negative least squares (NNLS) spectral modeling (136,159,160). NNLS presents an alternative to the rigid model fitting approaches. It does not

require *a priori* assumptions on the number of components of the signal decay nor starting parameters. This advantage can be particularly beneficial when evaluating renal pathologies in which the number of diffusion compartments or sources is not known in advance or might change during the disease progression or treatment. Although promising, these novel approaches should be validated in larger clinical studies and patients with various renal pathologies.

3.e Renal tissue characterization: virtual MR biopsy

The identification of MRI markers with a strong correlation to tissue histopathology is essential for establishing MRI as a non-invasive, "virtual" biopsy approach for the assessment of renal structure and functions. This section focuses on renal MRI studies that showed a direct correlation with tissue fibrosis, inflammation, glomerular or vascular dysfunction, as derived from qualitative or quantitative assessment of renal biopsy samples.

For "virtual biopsy" centered on MRI, investigations focus on identifying MRI markers that distinguish between degree of severity of pathological conditions such as fibrosis and inflammation, as reflected by the pathology scoring of traditional biopsy samples. Others have sought to correlate quantitative MRI markers with quantitative pathology metrics from tissue staining, such as the percentage tissue fraction stained for markers of fibrosis, such as Sirius red or Masson's trichrome (**Figure 7**). Thus, studies have established an association or negative correlation between either cortical ADC or corticomedullary difference in values (ΔADC) and interstitial fibrosis (IF) as measured by Banff scoring or Masson trichrome stain for native and transplanted kidneys (120,135,161,162). In human allografts, moderate negative correlation between cortical ADC and IF assessed by Masson trichrome stain, and corticomedullary difference in ADC values (ΔADC) correlated with eGFR and IF were reported (120,162,163). The inverse correlation of ADC with IF was significant (r=-0.77; $p<0.001$) in a study of 103 allografts with acute dysfunction undergoing indication biopsy, supporting the concept that DWI/ADC is useful when the study endpoint is IFTA, irrespective of other concomitant diagnoses (162). Corticomedullary ΔADC was found to be useful at separating high and low fibrosis as defined by the 40% tissue stained fraction for fibrosis, in both native (51) and transplanted kidneys (120).

T_1 relaxation measurements depend on both the molecular environment of the water molecules and the pathological changes occurring in the tissue (**Figure 7**), and have correlated with tissue fibrosis (due to the association of collagen) and inflammation (cellular swelling and interstitial edema). In a recent study including animal and human allografts, both T_1 and ADC values were correlated with IF and interstitial inflammation (120). Corticomedullary differences ΔADC and ΔT_1 were predictive of IF by Masson trichrome and Sirius red stain, but not inflammation (120). The combination of ΔADC and ΔT_1 showed improved performance for fibrosis detection by imaging variables alone, suggesting that the two

values measure slightly different processes (163). Human studies have confirmed significant associations for T_1 values and moderate/severe IF (AUC=0.76 for the diagnosis of interstitial fibrosis ci>1) and total inflammation (ti) (161). Corticomedullary ΔT_1 in combination with cortex ADC was found to distinguish stable allografts from allografts with chronic dysfunction and fibrosis with AUC=0.94 (164).

$T_{1\rho}$ is an emerging imaging marker for noninvasive assessment of renal fibrosis (165) (**Figure 7**). $T_1\rho$ is sensitive to the interactions between water molecules and macromolecules, including collagen. Only a few published studies have investigated $T_1\rho$ in the kidney, with an initial study showing increase in $T_1\rho$ relaxation time in patients with lupus nephritis compared to healthy controls, with very good/excellent measurement repeatability (166). A study in transplanted kidneys showed an AUC=0.77 of $T_1\rho$ for differentiating between functional allografts and chronic dysfunction with fibrosis (165). $T_1\rho$ may thus provide an indirect measurement of collagen deposition due to kidney fibrosis.

Magnetic resonance elastography (MRE) enables quantitative measurement of tissue stiffness by imaging the propagation of mechanical shear waves through tissue. MRE for the assessment of kidney fibrosis showed confounding results. Kennedy et al. reported that mean and median cortical MRE stiffness did not correlate with Banff scores, including ci+ct (167). Brown et al. showed that MRE renal stiffness decreased with CKD severity and fibrosis grade in a cohort of patients with DKD, with the decrease in stiffness mirroring decrease in renal perfusion, as measured concomitantly by ASL (168). Preliminary results indicate that MRE-derived stiffness is *not* solely or even dominantly dependent on renal interstitial fibrosis (169,170) and is confounded by blood flow, complex renal physiology, anisotropic renal anatomy and low spatial resolution parametric maps (171,172). Further constraints of MRE include the need for external hardware and specialized software, limiting widespread availability.

While most studies focus on the dyad of fibrosis and inflammation in the kidney, there has been interest in correlating IVIM-DWI parameters with Banff scores of vasculopathy, glomerulitis and peritubular capillary density (ptc) in transplants (164), and of ASL perfusion with ptc (162). MRI parameters have been combined with biopsy scores in models for the prediction of kidney transplant loss or re-listing at 2 years, emphasizing the complementary nature of quantitative MRI and traditional biopsy (164).

Last but not least, novel “virtual biopsy” applications in the kidneys have focused on direct quantification of nephron (glomeruli) number in-vivo in animals and in ex-vivo human kidneys, as the nephron constitutes the smallest functional unit in the kidney. Nephron number associates with CKD risk. Nephron quantification and single nephron GFR determination may allow for improved CKD progression risk assessment beyond GFR (173). Typically, nephron number in clinical studies is estimated by extrapolating the glomerular density measured on traditional patient biopsy samples, to the patient’s entire renal volume as measured by CT or MRI (174). Bennet et al. developed a method of measuring

nephron number by cationic-ferritin-enhanced MRI *in vivo* in animals and in ex-vivo human kidneys (175). This is a major leap since there is no preferred sampling location for biopsy and as many as 200 core needle biopsies would be needed to estimate kidney nephron number within 20% of the ground truth nephron number measured by cationic-ferritin enhanced MRI, with 95% confidence (176). While cationic ferritin MRI quantification of nephron number remains an ex-vivo and pre-clinical application, radiolabed cationic ferritin makes in-vivo nephron number quantification with PET(-MRI) a possibility in humans (177).

As previously mentioned, kidney macrophage infiltration, in addition to reduction in nephron number, portends poor prognosis in several kidney diseases. Hence, quantification of macrophage density from histopathology may soon be integrated into clinical practice (6). For the past 25 years, MRI with ultra-small paramagnetic iron oxide (USPIO) contrast agents that are phagocytosed by macrophages has been proposed for the non-invasive assessment of macrophage distribution in animal models of transplant rejection (178) or renal disease (179,180). T_2* in the organ of interest is measured before, early (4h) and 20-24 hrs after administration of a USPIO contrast agent, to allow for macrophage uptake of the USPIO(181). T_2* is expected to decrease in areas of high USPIO and macrophage concentration. Translation of these pre-clinical findings to a study of renal transplant rejection in children found that USPIO-enhanced T_2* was higher in allografts with acute rejection than without rejection, while there were no significant differences in macrophage concentration on histopathology between the two groups (181). Elevated T_2* in the allografts with rejection was likely due to decreased perfusion and increased edema (181). This suggests that USPIO-enhanced T_2* mapping has similar limitations as BOLD MRI, possibly remediated by other quantitative methods such as QSM. Macrophage quantification by MRI with or without iron oxides or other macrophage-labeling contrast agents remains an open area of investigation. Novel approaches of imaging the deleterious role of phagocytes such as monocytes, neutrophils and dendritic cells in the progression of kidney disease include explorations into ^{19}F MRI of the kidney, which represents an instrumental tool for the quantification of exogenous ^{19}F substances in vivo. ^{19}F MRI is commonly used in association with an intravenous administration of perfluorocarbons labelling of inflammatory cells - typically in nanoparticle form emulsions - to study the distribution of inflammatory cells that are migrating through the systemic circulation into inflamed organs in vivo (182).

3.f. Limitations of kidney MRI

Technical challenges and related confounding factors of MRI methods necessitate devoted efforts to advance the field. For example, some MRI methods like T_1 mapping do not distinguish inflammation and edema from fibrosis. In the assessment of kidney fibrosis, MRE and DWI are confounded by tissue perfusion. As mentioned above, MRE is currently limited in terms of spatial resolution to image the

anisotropic renal anatomy and complex renal physiology (171,172). Furthermore, BOLD remains sensitive to the effects of perfusion and to changes in kidney size. Finally, as with any biomarkers, age, sex and race-related effects may influence renal MRI parameters (183). Other limitations should also be recognized. While the possibilities outlined above for the characterization of renal tissue in terms of structure and function by MRI are exciting to clinicians, MRI is an expensive imaging modality, available mostly in urban centers in middle- and high-income countries. Expertise in renal functional MRI is available only at tertiary medical care facilities. In addition to its high cost and low availability, pulse sequence implementations and protocol parameters for the MRI techniques presented vary among vendors and research centers. For most of the techniques presented, there is an unmet need for standardization and harmonization of protocols among sites and vendors.

4. Recent advancements and future directions in kidney MRI

Some of the limitations of renal MRI overviewed above can be partially overcome by new hardware and software developments in MRI. Imaging at 7T can substantially increase SNR compared to 3T and 1.5T, which allows faster acquisition times or higher spatial resolution. Recent developments in transmit-receive RF coils have made human abdominal imaging at 7T a possibility (184). Although anatomical imaging of the kidney at 7T remains challenging because of inhomogeneities of the radiofrequency field and SAR constraints, a few studies have shown promising results in functional imaging (184,185). Renal BOLD at 7T benefits from increased susceptibility effects: renal BOLD studies at 7T (186-188) found higher R_2* values compared to 3T (although cortico-medullary R_2* ratios were roughly the same), and more pronounced decrease in medullary R_2* following a water loading challenge (188). ASL at 7T benefits from longer T_1 relaxation times (186), which allowed longer total delay time (1200 ms) between the inversion pulse and acquisition time, without loss of perfusion SNR, in a feasibility study of single-breath-hold kidney ASL(189).

In addition to hardware developments that can increase SNR, software developments in acquisition and post-processing can decrease imaging time while maintaining the quality of the data and the accuracy of quantitative parameters. Accelerated imaging through under-sampling, combined with compressed-sensing reconstruction is a means of obtaining high-quality anatomical images with high spatial resolution and reduced acquisition times. Compressed sensing combined with use of radial trajectories allowed free-breathing, high-spatial resolution T_1-weighted imaging for DCE-MRI and T_1 mapping in abdominal applications (190,191). However, compressed sensing reconstruction settings designed to reduce artifacts can also over-smooth the signal temporally, which reduces the accuracy of functional parameter mapping in techniques such as DCE-MRI (192). Use of deep learning image

reconstruction methods allows optimization of the reconstruction to maintain accuracy of DCE-MRI parameter estimation, while reducing artifacts (192).

5. Conclusions

This review provides a synopsis of the member-initiated symposium on renal MRI at ISMRM 2022. It summarizes state-of-the art technology, research directions, and applications of renal MRI. This survey reiterates that renal MRI has gone well beyond nascent stages of feasibility. The state of the field has evolved sufficiently, with accompanying evidence accumulation at the preclinical and clinical levels, to more deeply interrogate MRI markers of renal function. One source of deeper understanding comes in the form of more detailed models of each MRI technique (QSM, IVIM, etc), while another source of validation comes in comprehensive correlation with clinical standards of histopathology, physiology, and nephrology. Taken together, this body of work addresses the fundamental questions of the links between surrogate renal MRI markers, molecular profiles, biochemical markers and the signatures from physiological gold standard measurements, as well as what these relationships can tell us about the stages and evolution of kidney diseases over time, and responses to therapy and intervention. With these answers MRI adds value to patient management, as supplement or alternative to established standards such as serum eGFR and renal biopsy, and may ultimately provide markers to inform on the different stages of renal pathophysiology, improve prediction and interception of disease progression and evaluate treatment of renal disease.

REFERENCES

1. Collaboration GBDCKD. Global, regional, and national burden of chronic kidney disease, 1990-2017: a systematic analysis for the Global Burden of Disease Study 2017. Lancet 2020;395(10225):709-733.

2. Agency EM. Qualification opinion: Total Kidney Volume (TKV) as a prognostic biomarker for use in clinical trials evaluating patients with Autosomal Dominant Polycystic Kidney Disease. 2015.

3. Administration USFaD. Qualification of Biomarker Total Kidney Volume in Studies for Treatment of Autosomal Dominant Polycystic Kidney Disease Draft Guidance for Industry. 2016.

4. Abumoawad A, Saad A, Ferguson CM, et al. Tissue hypoxia, inflammation, and loss of glomerular filtration rate in human atherosclerotic renovascular disease. Kidney Int 2019;95(4):948-957.

5. Li L, Fu H, Liu Y. The fibrogenic niche in kidney fibrosis: components and mechanisms. Nat Rev Nephrol 2022;18(9):545-557.

6. Pfenning MB, Schmitz J, Scheffner I, et al. High Macrophage Densities in Native Kidney Biopsies Correlate With Renal Dysfunction and Promote ESRD. Kidney Int Rep 2023;8(2):341-356.

7. Bane O, Mendichovszky IA, Milani B, et al. Consensus-based technical recommendations for clinical translation of renal BOLD MRI. Magma 2020;33(1):199-215.

8. de Boer A, Villa G, Bane O, et al. Consensus-Based Technical Recommendations for Clinical Translation of Renal Phase Contrast MRI. J Magn Reson Imaging 2022;55(2):323-335.

9. Ljimani A, Caroli A, Laustsen C, et al. Consensus-based technical recommendations for clinical translation of renal diffusion-weighted MRI. Magma (New York, Ny) 2020;33(1):177-195.

10. Nery F, Buchanan CE, Harteveld AA, et al. Consensus-based technical recommendations for clinical translation of renal ASL MRI. Magma 2020;33(1):141-161.

11. Dekkers IA, de Boer A, Sharma K, et al. Consensus-based technical recommendations for clinical translation of renal T1 and T2 mapping MRI. Magma (New York, NY) 2020;33(1):163-176.

12. Mendichovszky I, Pullens P, Dekkers I, et al. Technical recommendations for clinical translation of renal MRI: a consensus project of the Cooperation in Science and Technology Action PARENCHIMA. Magma (New York, NY) 2020;33(1):131-140.

13. Pohlmann A, Back SJ, Fekete A, et al. Recommendations for Preclinical Renal MRI: A Comprehensive Open-Access Protocol Collection to Improve Training, Reproducibility, and Comparability of Studies. Methods Mol Biol 2021;2216:3-23.

14. Hall JE. Urine Formtion by the Kidney. In: Hall JE, ed. Guyton & Hall Textbook of Medical Physiology 12 ed. Philadelphia: Saunders Elsevier, 2011; 303-340.

15. Gardiner BS, Smith DW, Lee CJ, Ngo JP, Evans RG. Renal oxygenation: From data to insight. Acta Physiol (Oxf) 2020;228(4):e13450.

16. Cantow K, Evans RG, Grosenick D, et al. Quantitative Assessment of Renal Perfusion and Oxygenation by Invasive Probes: Basic Concepts. Methods Mol Biol 2021;2216:89-107.

17. Scholz H, Boivin FJ, Schmidt-Ott KM, et al. Kidney physiology and susceptibility to acute kidney injury: implications for renoprotection. Nat Rev Nephrol 2021;17(5):335-349.

18. Fähling M, Seeliger E, Patzak A, Persson PB. Understanding and preventing contrast-induced acute kidney injury. NatRevNephrol 2017;13(3):169-180.

19. Hultstrom M, Becirovic-Agic M, Jonsson S. Comparison of acute kidney injury of different etiology reveals in-common mechanisms of tissue damage. Physiological genomics 2018;50(3):127-141.

20. Seeliger E, Wronski T, Ladwig M, et al. The renin-angiotensin system and the third mechanism of renal blood flow autoregulation. AmJPhysiol Renal Physiol 2009;296(6):F1334-F1345.

21. Evans RG, Ince C, Joles JA, et al. Haemodynamic influences on kidney oxygenation: The clinical implications of integrative physiology. Clin Exp PharmacolPhysiol 2013;40:106-122.

22. Ma S, Evans RG, Iguchi N, et al. Sepsis-induced acute kidney injury: A disease of the microcirculation. Microcirculation (New York, NY : 1994) 2019;26(2):e12483.

23. Hansell P, Welch WJ, Blantz RC, Palm F. Determinants of kidney oxygen consumption and their relationship to tissue oxygen tension in diabetes and hypertension. ClinExpPharmacolPhysiol 2013;40(2):123-137.

24. Herrler T, Tischer A, Meyer A, et al. The intrinsic renal compartment syndrome: new perspectives in kidney transplantation. Transplantation 2010;89(1):40-46.

25. Gladytz T, Millward JM, Cantow K, et al. Reliable Kidney Size Determination by Magnetic Resonance Imaging in Pathophysiological Settings. Acta Physiol (Oxf) 2021;233:e13701.

26. Cantow K, Gladytz T, Millward JM, Waiczies S, Niendorf T, Seeliger E. Monitoring kidney size to interpret MRI-based assessment of renal oxygenation in acute pathophysiological scenarios. Acta Physiol (Oxf) 2023;237:e13868.

27. Li LP, Hack B, Seeliger E, Prasad PV. MRI Mapping of the Blood Oxygenation Sensitive Parameter T(2)* in the Kidney: Basic Concept. Methods Mol Biol 2021;2216:171-185.

28. Niendorf T, Seeliger E, Cantow K, Flemming B, Waiczies S, Pohlmann A. Probing renal blood volume with magnetic resonance imaging. Acta Physiol (Oxf) 2020;228(4):e13435.

29. Pohlmann A, Arakelyan K, Hentschel J, et al. Detailing the relation between renal T2* and renal tissue pO2 using an integrated approach of parametric magnetic resonance imaging and invasive physiological measurements. Invest Radiol 2014;49(8):547-560.

30. Niendorf T, Pohlmann A, Arakelyan K, et al. How bold is blood oxygenation level-dependent (BOLD) magnetic resonance imaging of the kidney? Opportunities, challenges and future directions. Acta Physiol (Oxf) 2015;213(1):19-38.

31. Azawi N, Jensen M, Jensen BL, Goetze JP, Bistrup C, Lund L. Functional adaptation after kidney tissue removal in patients is associated with increased plasma atrial natriuretic peptide concentration. Nephrol Dial Transplant 2022(37):2138-2149.

32. Tokas T, Herrmann TRW, Skolarikos A, Nagele U. Pressure matters: intrarenal pressures during normal and pathological conditions, and impact of increased values to renal physiology. World J Urol 2019;37(1):125-131.

33. Reinhardt HW, Seeliger E. Toward an integrative concept of control of total body sodium. News PhysiolSci 2000;15(6):319-325.

34. Sato Y, Yanagita M. Immune cells and inflammation in AKI to CKD progression. Am J Physiol Renal Physiol 2018;315(6):F1501-f1512.

35. Thomas HY, Ford Versypt AN. Pathophysiology of mesangial expansion in diabetic nephropathy: mesangial structure, glomerular biomechanics, and biochemical signaling and regulation. J Biol Eng 2022;16(1):19.

36. van Duijl TT, Soonawala D, de Fijter JW, Ruhaak LR, Cobbaert CM. Rational selection of a biomarker panel targeting unmet clinical needs in kidney injury. Clin Proteomics 2021;18(1):10.

37. Porrini E, Ruggenenti P, Luis-Lima S, et al. Estimated GFR: time for a critical appraisal. Nat Rev Nephrol 2019;15(3):177-190.

38. Caroli A, Remuzzi A, Remuzzi G. Does MRI trump pathology? A new era for staging and monitoring of kidney fibrosis. Kidney Int 2020;97(3):442-444.

39. Molitoris BA. Urinary Biomarkers: Alone Are They Enough? JAmSocNephrol 2015;26(7):1485-1488.

40. Niendorf T, Pohlmann A, Arakelyan K, et al. How bold is blood oxygenation level-dependent (BOLD) magnetic resonance imaging of the kidney? Opportunities, challenges and future directions. Acta Physiol (Oxf) 2015;213(1):19-38.

41. Selby NM, Blankestijn PJ, Boor P, et al. Magnetic resonance imaging biomarkers for chronic kidney disease: a position paper from the European Cooperation in Science and Technology Action PARENCHIMA. Nephrol Dial Transplant 2018;33(suppl_2):ii4-ii14.

42. Simms R, Sourbron S. Recent findings on the clinical utility of renal magnetic resonance imaging biomarkers. Nephrol Dial Transplant 2020;35(6):915-919.

43. Luciano RL, Moeckel GW. Update on the Native Kidney Biopsy: Core Curriculum 2019. Am J Kidney Dis 2019;73(3):404-415.

44. Loupy A, Haas M, Roufosse C, et al. The Banff 2019 Kidney Meeting Report (I): Updates on and clarification of criteria for T cell- and antibody-mediated rejection. Am J Transplant 2020;20(9):2318-2331.

45. Seron D, Moreso F, Fulladosa X, Hueso M, Carrera M, Grinyo JM. Reliability of chronic allograft nephropathy diagnosis in sequential protocol biopsies. Kidney Int 2002;61(2):727-733.

46. Furness PN, Philpott CM, Chorbadjian MT, et al. Protocol biopsy of the stable renal transplant: a multicenter study of methods and complication rates. Transplantation 2003;76(6):969-973.

47. Elshafie M, Furness PN. Identification of lesions indicating rejection in kidney transplant biopsies: tubulitis is severely under-detected by conventional microscopy. Nephrol Dial Transplant 2012;27(3):1252-1255.

48. Poggio ED, McClelland RL, Blank KN, et al. Systematic Review and Meta-Analysis of Native Kidney Biopsy Complications. Clin J Am Soc Nephrol 2020;15(11):1595-1602.

49. Ho QY, Lim CC, Tan HZ, Sultana R, Kee T, Htay H. Complications of Percutaneous Kidney Allograft Biopsy: Systematic Review and Meta-analysis. Transplantation 2022;106(7):1497-1506.

50. Baffour FI, Hickson LJ, Stegall MD, et al. Effects of Aspirin Therapy on Ultrasound-Guided Renal Allograft Biopsy Bleeding Complications. J Vasc Interv Radiol 2017;28(2):188-194.

51. Buchanan CE, Mahmoud H, Cox EF, et al. Quantitative assessment of renal structural and functional changes in chronic kidney disease using multi-parametric magnetic resonance imaging. Nephrol Dial Transplant 2020;35(6):955-964.

52. Magistroni R, Corsi C, Martí T, Torra R. A Review of the Imaging Techniques for Measuring Kidney and Cyst Volume in Establishing Autosomal Dominant Polycystic Kidney Disease Progression. Am J Nephrol 2018;48(1):67-78.

53. Grantham JJ, Torres VE. The importance of total kidney volume in evaluating progression of polycystic kidney disease. Nat Rev Nephrol 2016;12(11):667-677.

54. Kline TL, Edwards ME, Fetzer J, et al. Automatic semantic segmentation of kidney cysts in MR images of patients affected by autosomal-dominant polycystic kidney disease. Abdom Radiol (NY) 2021;46(3):1053-1061.

55. Goel A, Shih G, Riyahi S, et al. Deployed Deep Learning Kidney Segmentation for Polycystic Kidney Disease MRI. Radiol Artif Intell 2022;4(2):e210205.

56. Raj A, Tollens F, Hansen L, et al. Deep Learning-Based Total Kidney Volume Segmentation in Autosomal Dominant Polycystic Kidney Disease Using Attention, Cosine Loss, and Sharpness Aware Minimization. Diagnostics (Basel) 2022;12(5).

57. Langner T, Östling A, Maldonis L, et al. Kidney segmentation in neck-to-knee body MRI of 40,000 UK Biobank participants. Sci Rep 2020;10(1):20963.

58. Kart T, Fischer M, Winzeck S, et al. Automated imaging-based abdominal organ segmentation and quality control in 20,000 participants of the UK Biobank and German National Cohort Studies. Sci Rep 2022;12(1):18733.

59. Daniel AJ, Buchanan CE, Allcock T, et al. Automated renal segmentation in healthy and chronic kidney disease subjects using a convolutional neural network. Magn Reson Med 2021;86(2):1125-1136.

60. Aslam I, Aamir F, Kassai M, et al. Validation of automatically measured T1 map cortico-medullary difference (ΔT1) for eGFR and fibrosis assessment in allograft kidneys. PLoS One 2023;18(2):e0277277.

61. Bak M, Thomsen K, Christiansen T, Flyvbjerg A. Renal enlargement precedes renal hyperfiltration in early experimental diabetes in rats. J Am Soc Nephrol 2000;11(7):1287-1292.

62. Erokwu BO, Anderson CE, Flask CA, Dell KM. Quantitative magnetic resonance imaging assessments of autosomal recessive polycystic kidney disease progression and response to therapy in an animal model. Pediatr Res 2018;83(5):1067-1074.

63. Hueper K, Hensen B, Gutberlet M, et al. Kidney Transplantation: Multiparametric Functional Magnetic Resonance Imaging for Assessment of Renal Allograft Pathophysiology in Mice. Invest Radiol 2016;51(1):58-65.

64. Pohlmann A, Zhao K, Fain SB, Prasad PV, Niendorf T. Experimental Protocol for MRI Mapping of the Blood Oxygenation-Sensitive Parameters T(2)* and T(2) in the Kidney. Methods Mol Biol 2021;2216:403-417.

65. Cantow K, Ladwig-Wiegard M, Flemming B, Pohlmann A, Niendorf T, Seeliger E. Monitoring Renal Hemodynamics and Oxygenation by Invasive Probes: Experimental Protocol. Methods Mol Biol 2021;2216:327-347.

66. Cantow K, Ladwig-Wiegard M, Flemming B, Fekete A, Hosszu A, Seeliger E. Reversible (Patho)Physiologically Relevant Test Interventions: Rationale and Examples. Methods Mol Biol 2021;2216:57-73.

67. Seeliger E, Cantow K, Arakelyan K, Ladwig M, Persson PB, Flemming B. Low-Dose Nitrite Alleviates Early Effects of an X-ray Contrast Medium on Renal Hemodynamics and Oxygenation in Rats. Invest Radiol 2014;49:70-77.

68. Michaely HJ, Metzger L, Haneder S, Hansmann J, Schoenberg SO, Attenberger UI. Renal BOLD-MRI does not reflect renal function in chronic kidney disease. Kidney Int 2012;81(7):684-689.

69. Pruijm M, Hofmann L, Piskunowicz M, et al. Determinants of renal tissue oxygenation as measured with BOLD-MRI in chronic kidney disease and hypertension in humans. PLoSONE 2014;9(4):e95895.

70. Milani B, Ansaloni A, Sousa-Guimaraes S, et al. Reduction of cortical oxygenation in chronic kidney disease: evidence obtained with a new analysis method of blood oxygenation level-dependent magnetic resonance imaging. Nephrol Dial Transplant 2017;32(12):2097–2105.

71. Fine LG, Dharmakumar R. Limitations of BOLD-MRI for assessment of hypoxia in chronically diseased human kidneys. Kidney Int 2012;82(8):934-935.

72. Prasad PV, Thacker J, Li LP, et al. Multi-Parametric Evaluation of Chronic Kidney Disease by MRI: A Preliminary Cross-Sectional Study. PLoSONE 2015;10(10):e0139661.

73. Pruijm M, Mendichovszky IA, Liss P, et al. Renal blood oxygenation level-dependent magnetic resonance imaging to measure renal tissue oxygenation: a statement paper and systematic review. Nephrol Dial Transplant 2018;33(suppl_2):ii22-ii28.

74. Pruijm M, Milani B, Pivin E, et al. Reduced cortical oxygenation predicts a progressive decline of renal function in patients with chronic kidney disease. Kidney Int 2018;93(4):932-940.

75. Han F, Xiao W, Xu Y, et al. The significance of BOLD MRI in differentiation between renal transplant rejection and acute tubular necrosis. Nephrol Dial Transplant 2008;23(8):2666-2672.

76. Djamali A, Sadowski EA, Samaniego-Picota M, et al. Noninvasive assessment of early kidney allograft dysfunction by blood oxygen level-dependent magnetic resonance imaging. Transplantation 2006;82(5):621-628.

77. Abumoawad A, Saad A, Ferguson CM, et al. In a Phase 1a escalating clinical trial, autologous mesenchymal stem cell infusion for renovascular disease increases blood flow and the glomerular filtration rate while reducing inflammatory biomarkers and blood pressure. Kidney Int 2020;97(4):793-804.

78. Cantow K, Arakelyan K, Seeliger E, Niendorf T, Pohlmann A. Assessment of Renal Hemodynamics and Oxygenation by Simultaneous Magnetic Resonance Imaging (MRI) and Quantitative Invasive Physiological Measurements. Methods Mol Biol 2016;1397:129-154.

79. Pohlmann A, Cantow K, Hentschel J, et al. Linking non-invasive parametric MRI with invasive physiological measurements (MR-PHYSIOL): towards a hybrid and integrated approach for investigation of acute kidney injury in rats. Acta Physiol (Oxf) 2013;207(4):673-689.

80. Bechler E, Stabinska J, Thiel T, et al. Feasibility of quantitative susceptibility mapping (QSM) of the human kidney. MAGMA 2021;34(3):389-397.

81. Pruijm M, Milani B, Burnier M. Blood Oxygenation Level-Dependent MRI to Assess Renal Oxygenation in Renal Diseases: Progresses and Challenges. Front Physiol 2016;7:667.

82. Ravanfar P, Loi SM, Syeda WT, et al. Systematic Review: Quantitative Susceptibility Mapping (QSM) of Brain Iron Profile in Neurodegenerative Diseases. Front Neurosci 2021;15:618435.

83. Wang Y, Liu T. Quantitative susceptibility mapping (QSM): Decoding MRI data for a tissue magnetic biomarker. Magnetic Resonance in Medicine 2015;73:82-101.

84. Robinson SD, Bredies K, Khabipova D, Dymerska B, Marques JP, Schweser F. An illustrated comparison of processing methods for MR phase imaging and QSM: combining array coil signals and phase unwrapping. NMR in Biomedicine 2017;30:e3601.

85. Schweser F, Robinson SD, de Rochefort L, Li W, Bredies K. An illustrated comparison of processing methods for phase MRI and QSM: removal of background field contributions from sources outside the region of interest. NMR in Biomedicine 2017;30:e3604.

86. Bilgic B, Langkammer C, Marques JP, Meineke J, Milovic C, Schweser F. QSM reconstruction challenge 2.0: Design and report of results. Magnetic Resonance in Medicine 2021;86:1241-1255.

87. Xie L, Sparks MA, Li W, et al. Quantitative susceptibility mapping of kidney inflammation and fibrosis in type 1 angiotensin receptor-deficient mice. NMR in Biomedicine 2013;26:1853-1863.

88. Luo J, He X, D'Avignon DA, Ackerman JJH, Yablonskiy DA. Protein-induced water 1H MR frequency shifts: Contributions from magnetic susceptibility and exchange effects. Journal of Magnetic Resonance 2010;202:102-108.

89. Villa G, Ringgaard S, Hermann I, et al. Phase-contrast magnetic resonance imaging to assess renal perfusion: a systematic review and statement paper. Magma 2020;33(1):3-21.

90. Motoyama D, Ishii Y, Takehara Y, et al. Four-dimensional phase-contrast vastly undersampled isotropic projection reconstruction (4D PC-VIPR) MR evaluation of the renal arteries in transplant recipients: Preliminary results. J Magn Reson Imaging 2017;46(2):595-603.

91. Bane O, Said D, Weiss A, et al. 4D flow MRI for the assessment of renal transplant dysfunction: initial results. Eur Radiol 2021;31(2):909-919.

92. Zhang JL. Functional Magnetic Resonance Imaging of the Kidneys-With and Without Gadolinium-Based Contrast. Adv Chronic Kidney Dis 2017;24(3):162-168.

93. de Boer A, Harteveld AA, Stemkens B, et al. Multiparametric Renal MRI: An Intrasubject Test-Retest Repeatability Study. J Magn Reson Imaging 2021;53(3):859-873.

94. Eikefjord E, Andersen E, Hodneland E, et al. Dynamic contrast-enhanced MRI measurement of renal function in healthy participants. Acta Radiol 2017;58(6):748-757.

95. Buchanan CE, Cox EF, Francis ST. Evaluation of 2D Imaging Schemes for Pulsed Arterial Spin Labeling of the Human Kidney Cortex. Diagnostics (Basel) 2018;8(3).

96. Gardener AG, Francis ST. Multislice perfusion of the kidneys using parallel imaging: image acquisition and analysis strategies. Magn Reson Med 2010;63(6):1627-1636.

97. Harteveld AA, de Boer A, Franklin SL, Leiner T, van Stralen M, Bos C. Comparison of multi-delay FAIR and pCASL labeling approaches for renal perfusion quantification at 3T MRI. Magma 2020;33(1):81-94.

98. Taso M, Guidon A, Alsop DC. Influence of background suppression and retrospective realignment on free-breathing renal perfusion measurement using pseudo-continuous ASL. Magn Reson Med 2019;81(4):2439-2449.

99. Liss P, Cox EF, Eckerbom P, Francis ST. Imaging of intrarenal haemodynamics and oxygen metabolism. Clin Exp Pharmacol Physiol 2013;40(2):158-167.

100. Francis ST, Bowtell R, Gowland PA. Modeling and optimization of Look-Locker spin labeling for measuring perfusion and transit time changes in activation studies taking into account arterial blood volume. Magn Reson Med 2008;59(2):316-325.

101. Cox EF, Buchanan CE, Bradley CR, et al. Multiparametric Renal Magnetic Resonance Imaging: Validation, Interventions, and Alterations in Chronic Kidney Disease. Front Physiol 2017;8:696.

102. Odudu A, Nery F, Harteveld AA, et al. Arterial spin labelling MRI to measure renal perfusion: a systematic review and statement paper. Nephrol Dial Transplant 2018;33(suppl_2):ii15-ii21.

103. Nery F, Gordon I, Thomas DL. Non-Invasive Renal Perfusion Imaging Using Arterial Spin Labeling MRI: Challenges and Opportunities. Diagnostics (Basel) 2018;8(1).

104. Cutajar M, Thomas DL, Hales PW, Banks T, Clark CA, Gordon I. Comparison of ASL and DCE MRI for the non-invasive measurement of renal blood flow: quantification and reproducibility. Eur Radiol 2014;24(6):1300-1308.

105. Alhummiany BA, Shelley D, Saysell M, et al. Bias and Precision in Magnetic Resonance Imaging-Based Estimates of Renal Blood Flow: Assessment by Triangulation. J Magn Reson Imaging 2022;55(4):1241-1250.

106. Hueper K, Gueler F, Bräsen JH, et al. Functional MRI detects perfusion impairment in renal allografts with delayed graft function. Am J Physiol Renal Physiol 2015;308(12):F1444-1451.

107. Breidthardt T, Cox EF, Squire I, et al. The pathophysiology of the chronic cardiorenal syndrome: a magnetic resonance imaging study. Eur Radiol 2015;25(6):1684-1691.

108. Heusch P, Wittsack HJ, Blondin D, et al. Functional evaluation of transplanted kidneys using arterial spin labeling MRI. J Magn Reson Imaging 2014;40(1):84-89.

109. Ren T, Wen CL, Chen LH, et al. Evaluation of renal allografts function early after transplantation using intravoxel incoherent motion and arterial spin labeling MRI. Magn Reson Imaging 2016;34(7):908-914.

110. Li LP, Tan H, Thacker JM, et al. Evaluation of Renal Blood Flow in Chronic Kidney Disease Using Arterial Spin Labeling Perfusion Magnetic Resonance Imaging. Kidney Int Rep 2017;2(1):36-43.

111. Shimizu K, Kosaka N, Fujiwara Y, et al. Arterial Transit Time-corrected Renal Blood Flow Measurement with Pulsed Continuous Arterial Spin Labeling MR Imaging. Magn Reson Med Sci 2017;16(1):38-44.

112. Dujardin M, Luypaert R, Sourbron S, Verbeelen D, Stadnik T, de Mey J. Age dependence of T1 perfusion MRI-based hemodynamic parameters in human kidneys. J Magn Reson Imaging 2009;29(2):398-403.

113. Echeverria-Chasco R, Vidorreta M, Aramendía-Vidaurreta V, et al. Optimization of pseudo-continuous arterial spin labeling for renal perfusion imaging. Magn Reson Med 2021;85(3):1507-1521.

114. Khatir DS, Pedersen M, Jespersen B, Buus NH. Evaluation of Renal Blood Flow and Oxygenation in CKD Using Magnetic Resonance Imaging. Am J Kidney Dis 2015;66(3):402-411.

115. Buchanan C, Mahmoud H, Cox E, et al. Multiparametric MRI assessment of renal structure and function in acute kidney injury and renal recovery. Clin Kidney J 2021;14(8):1969-1976.

116. Dong J, Yang L, Su T, et al. Quantitative assessment of acute kidney injury by noninvasive arterial spin labeling perfusion MRI: a pilot study. Science China Life sciences 2013;56(8):745-750.

117. Prowle JR, Molan MP, Hornsey E, Bellomo R. Measurement of renal blood flow by phase-contrast magnetic resonance imaging during septic acute kidney injury: a pilot investigation. Crit Care Med 2012;40(6):1768-1776.

118. Luther T, Eckerbom P, Cox E, et al. Decreased renal perfusion during acute kidney injury in critical COVID-19 assessed by magnetic resonance imaging: a prospective case control study. Crit Care 2022;26(1):262.

119. Inoue T, Kozawa E, Okada H, et al. Noninvasive Evaluation of Kidney Hypoxia and Fibrosis Using Magnetic Resonance Imaging. Journal of the American Society of Nephrology : JASN 2011;22(8):1429-1434.

120. Friedli I, Crowe LA, Berchtold L, et al. New Magnetic Resonance Imaging Index for Renal Fibrosis Assessment: A Comparison between Diffusion-Weighted Imaging and T1 Mapping with Histological Validation. Scientific Reports 2016;6:30088.

121. Park SY, Kim CK, Park BK, Kim SJ, Lee S, Huh W. Assessment of early renal allograft dysfunction with blood oxygenation level-dependent MRI and diffusion-weighted imaging. European Journal of Radiology 2014;83(12):2114-2121.

122. Faletti R, Cassinis MC, Fonio P, et al. Diffusion–Weighted Imaging and Apparent Diffusion Coefficient Values Versus Contrast–Enhanced MR Imaging in the Identification and Characterisation of Acute Pyelonephritis. European Radiology 2013;23(12):3501-3508.

123. Thoeny HC, De Keyzer F. Diffusion-weighted MR Imaging of Native and Transplanted Kidneys. Radiology 2011;259(1):25-38.

124. Suwabe T, Ubara Y, Ueno T, et al. Intracystic magnetic resonance imaging in patients with autosomal dominant polycystic kidney disease: features of severe cyst infection in a case–control study. BMC Nephrology 2016;17:170.

125. Thoeny HC, Binser T, Roth B, Kessler TM, Vermathen P. Noninvasive Assessment of Acute Ureteral Obstruction with Diffusion-weighted MR Imaging: A Prospective Study. Radiology 2009;252(3):721-728.

126. Yildirim E, Kirbas I, Teksam M, Karadeli E, Gullu H, Ozer I. Diffusion-weighted MR imaging of kidneys in renal artery stenosis. European Journal of Radiology 2008;65(1):148-153.

127. Zhao J, Wang ZJ, Liu M, et al. Assessment of renal fibrosis in chronic kidney disease using diffusion-weighted MRI. Clinical Radiology 2014;69(11):1117-1122.

128. Xu X, Fang W, Ling H, Chai W, Chen K. Diffusion-weighted MR imaging of kidneys in patients with chronic kidney disease: initial study. European Radiology 2010;20(4):978-983.

129. Yalçin-Şafak K, Ayyildiz M, Ünel SY, Umarusman-Tanju N, Akça A, Baysal T. The relationship of ADC values of renal parenchyma with CKD stage and serum creatinine levels. European Journal of Radiology Open 2015;3:8-11.

130. Le Bihan D, Breton E, Lallemand D, Aubin ML, Vignaud J, Laval-Jeantet M. Separation of diffusion and perfusion in intravoxel incoherent motion MR imaging. Radiology 1988;168(2):497-505.

131. Zhang JL, Sigmund EE, Chandarana H, et al. Variability of Renal Apparent Diffusion Coefficients: Limitations of the Monoexponential Model for Diffusion Quantification. Radiology 2010;254(3):783-792.

132. Ichikawa S, Motosugi U, Ichikawa T, Sano K, Morisaka H, Araki T. Intravoxel incoherent motion imaging of the kidney: alterations in diffusion and perfusion in patients with renal dysfunction. Magnetic Resonance Imaging 2013;31(3):414-417.

133. Ebrahimi B, Rihal N, Woollard JR, Krier JD, Eirin A, Lerman LO. Assessment of renal artery stenosis using intravoxel incoherent motion diffusion-weighted magnetic resonance imaging analysis. Invest Radiol 2014;49(10):640-646.

134. Kim JW, Lee CH, Yoo KH, et al. Intravoxel incoherent motion magnetic resonance imaging to predict vesicoureteral reflux in children with urinary tract infection. Eur Radiol 2016;26(6):1670-1677.

135. Hueper K, Khalifa AA, Bräsen JH, et al. Diffusion-Weighted imaging and diffusion tensor imaging detect delayed graft function and correlate with allograft fibrosis in patients early after kidney transplantation. Journal of Magnetic Resonance Imaging 2016;44(1):112-121.

136. Stabinska J, Ljimani A, Zöllner HJ, et al. Spectral diffusion analysis of kidney intravoxel incoherent motion MRI in healthy volunteers and patients with renal pathologies. Magnetic Resonance in Medicine 2021;85(6):3085-3095.

137. van Baalen S, Leemans A, Dik P, Lilien MR, ten Haken B, Froeling M. Intravoxel incoherent motion modeling in the kidneys: Comparison of mono-, bi-, and triexponential fit. Journal of Magnetic Resonance Imaging 2017;46(1):228-239.

138. Caroli A, Schneider M, Friedli I, et al. Diffusion-weighted magnetic resonance imaging to assess diffuse renal pathology: a systematic review and statement paper. Nephrology Dialysis Transplantation 2018;33(Suppl 2):ii29-ii40.

139. Malyarenko DI, Newitt D, L JW, et al. Demonstration of nonlinearity bias in the measurement of the apparent diffusion coefficient in multicenter trials. Magn Reson Med 2016;75(3):1312-1323.

140. Wittsack H-J, Lanzman RS, Quentin M, et al. Temporally Resolved Electrocardiogram-Triggered Diffusion-Weighted Imaging of the Human Kidney: Correlation Between Intravoxel Incoherent Motion Parameters and Renal Blood Flow at Different Time Points of the Cardiac Cycle. Investigative Radiology 2012;47(4):226–230.

141. Sigmund EE, Mikheev A, Brinkmann IM, et al. Cardiac Phase and Flow Compensation Effects on REnal Flow and Microstructure AnisotroPy MRI in Healthy Human Kidney. J Magn Reson Imaging 2022.

142. Sigmund EE, Vivier P-H, Sui D, et al. Intravoxel incoherent motion and diffusion-tensor imaging in renal tissue under hydration and furosemide flow challenges. Radiology 2012;263(3):758-769.

143. Gaudiano C, Clementi V, Busato F, et al. Diffusion tensor imaging and tractography of the kidneys: assessment of chronic parenchymal diseases. European Radiology 2013;23(6):1678-1685.

144. Liu Z, Xu Y, Zhang J, et al. Chronic kidney disease: pathological and functional assessment with diffusion tensor imaging at 3T MR. European Radiology 2015;25(3):652-660.

145. Wang WJ, Pui MH, Guo Y, Wang LQ, Wang HJ, Liu M. 3T magnetic resonance diffusion tensor imaging in chronic kidney disease. Abdom Imaging 2014;39(4):770-775.

146. Lu L, Sedor JR, Gulani V, et al. Use of Diffusion Tensor MRI to Identify Early Changes in Diabetic Nephropathy. American Journal of Nephrology 2011;34(5):476-482.

147. Feng Q, Ma Z, Wu J, Fang W. DTI for the assessment of disease stage in patients with glomerulonephritis - correlation with renal histology. European Radiology 2015;25(1):92-98.

148. Fan W-j, Ren T, Li Q, et al. Assessment of renal allograft function early after transplantation with isotropic resolution diffusion tensor imaging. European Radiology 2016;26(2):567-575.

149. Lanzman RS, Ljimani A, Pentang G, et al. Kidney Transplant: Functional Assessment with Diffusion-Tensor MR Imaging at 3T. Radiology 2013;266(1):218-225.

150. Lupica R, Mormina E, Lacquaniti A, et al. 3 Tesla-Diffusion Tensor Imaging in Autosomal Dominant Polycystic Kidney Disease: The Nephrologist's Point of View. Nephron 2016;134(2):73-80.

151. Serai SD, Otero HJ, Calle-Toro JS, Berman JI, Darge K, Hartung EA. Diffusion tensor imaging of the kidney in healthy controls and in children and young adults with autosomal recessive polycystic kidney disease. Abdominal radiology (New York) 2019;44(5):1867-1872.

152. Cheng Z-Y, Feng Y-Z, Liu X-L, Ye Y-J, Hu J-J, Cai X-R. Diffusional kurtosis imaging of kidneys in patients with hyperuricemia: initial study. Acta Radiologica 2020;61(6):839-847.

153. Liu Y, Zhang G-m-y, Peng X, et al. Diffusional kurtosis imaging in assessing renal function and pathology of IgA nephropathy: a preliminary clinical study. Clinical Radiology 2018;73(9):818-826.

154. Mao W, Ding Y, Ding X, et al. Pathological assessment of chronic kidney disease with DWI: Is there an added value for diffusion kurtosis imaging? Journal of Magnetic Resonance Imaging 2021;54(2):508-517.

155. Notohamiprodjo M, Chandarana H, Mikheev A, et al. Combined intravoxel incoherent motion and diffusion tensor imaging of renal diffusion and flow anisotropy. Magnetic Resonance in Medicine 2015;73(4):1526-1532.

156. Hilbert F, Bock M, Neubauer H, et al. An intravoxel oriented flow model for diffusion-weighted imaging of the kidney. NMR in Biomedicine 2016;29(10):1403-1413.

157. Phi van V, Reiner CS, Klarhoefer M, et al. Diffusion tensor imaging of the abdominal organs: Influence of oriented intravoxel flow compartments. NMR in Biomedicine 2019;32(11):e4159.

158. Liu A, Mikheev A, Rusinek H, et al. REnal Flow and Microstructure AnisotroPy (REFMAP) magnetic resonance imaging in normal and peritumoral renal tissue. Journal of magnetic resonance imaging : JMRI 2018;48(1):188-197.

159. Wurnig MC, Germann M, Boss A. Is there evidence for more than two diffusion components in abdominal organs? – A magnetic resonance imaging study in healthy volunteers. NMR in Biomedicine 2018;31(1):e3852.

160. Periquito JS, Gladytz T, Millward JM, et al. Continuous diffusion spectrum computation for diffusion-weighted magnetic resonance imaging of the kidney tubule system. Quantitative Imaging in Medicine and Surgery 2021;11(7):3098-3119.

161. Andrea Beck-Tölly ME, Dietrich Beitzke, Farsad Eskandary, Asan Agibetov, Katharina Lampichler, Martina Hamböck, Heinz Regele, Johannes Kläger, Maja Nackenhorst, and Georg A. Böhmig. Magnetic Resonance Imaging for Evaluation of Interstitial Fibrosis in Kidney Allografts. Transplantation Direct 2020.

162. Wang W, Yu Y, Wen J, et al. Combination of Functional Magnetic Resonance Imaging and Histopathologic Analysis to Evaluate Interstitial Fibrosis in Kidney Allografts. Clin J Am Soc Nephrol 2019;14(9):1372-1380.

163. Berchtold L, Friedli I, Crowe LA, et al. Validation of the corticomedullary difference in magnetic resonance imaging-derived apparent diffusion coefficient for kidney fibrosis detection: a cross-sectional study. Nephrol Dial Transplant 2020;35(6):937-945.

164. Bane O, Hectors SJ, Gordic S, et al. Multiparametric magnetic resonance imaging shows promising results to assess renal transplant dysfunction with fibrosis. Kidney Int 2020;97(2):414-420.

165. Hectors SJ, Bane O, Kennedy P, et al. T1rho mapping for assessment of renal allograft fibrosis. J Magn Reson Imaging 2019.

166. Rapacchi S, Smith RX, Wang Y, et al. Towards the identification of multi-parametric quantitative MRI biomarkers in lupus nephritis. Magn Reson Imaging 2015;33(9):1066-1074.

167. Kennedy P, Bane O, Hectors SJ, et al. Magnetic resonance elastography vs. point shear wave ultrasound elastography for the assessment of renal allograft dysfunction. Eur J Radiol 2020;130:109180.

168. Brown RS, Sun MRM, Stillman IE, Russell TL, Rosas SE, Wei JL. The utility of magnetic resonance imaging for noninvasive evaluation of diabetic nephropathy. Nephrol Dial Transplant 2020;35(6):970-978.

169. Lee CU, Glockner JF, Glaser KJ, et al. MR elastography in renal transplant patients and correlation with renal allograft biopsy: a feasibility study. Acad Radiol 2012;19(7):834-841.

170. Marticorena Garcia SR, Fischer T, Durr M, et al. Multifrequency Magnetic Resonance Elastography for the Assessment of Renal Allograft Function. Invest Radiol 2016;51(9):591-595.

171. Streitberger KJ, Guo J, Tzschatzsch H, et al. High-resolution mechanical imaging of the kidney. J Biomech 2014;47(3):639-644.

172. Gennisson JL, Grenier N, Combe C, Tanter M. Supersonic shear wave elastography of in vivo pig kidney: influence of blood pressure, urinary pressure and tissue anisotropy. Ultrasound Med Biol 2012;38(9):1559-1567.

173. Denic A, Elsherbiny H, Rule AD. In-vivo techniques for determining nephron number. Current opinion in nephrology and hypertension 2019;28(6):545-551.

174. Denic A, Mathew J, Lerman LO, et al. Single-Nephron Glomerular Filtration Rate in Healthy Adults. N Engl J Med 2017;376(24):2349-2357.

175. Baldelomar EJ, Charlton JR, Beeman SC, et al. Phenotyping by magnetic resonance imaging nondestructively measures glomerular number and volume distribution in mice with and without nephron reduction. Kidney Int 2016;89(2):498-505.

176. Morozov D, Parvin N, Conaway M, et al. Estimating Nephron Number from Biopsies: Impact on Clinical Studies. J Am Soc Nephrol 2022;33(1):39-48.

177. Baldelomar EJ, Reichert DE, Shoghi KI, et al. Mapping nephron mass in vivo using positron emission tomography. Am J Physiol Renal Physiol 2021;320(2):F183-f192.

178. Ho C, Hitchens TK. A non-invasive approach to detecting organ rejection by MRI: monitoring the accumulation of immune cells at the transplanted organ. Curr Pharm Biotechnol 2004;5(6):551-566.

179. Rubio-Navarro A, Carril M, Padro D, et al. CD163-Macrophages Are Involved in Rhabdomyolysis-Induced Kidney Injury and May Be Detected by MRI with Targeted Gold-Coated Iron Oxide Nanoparticles. Theranostics 2016;6(6):896-914.

180. Luo B, Wen S, Chen YC, et al. LOX-1-Targeted Iron Oxide Nanoparticles Detect Early Diabetic Nephropathy in db/db Mice. Mol Imaging Biol 2015;17(5):652-660.

181. Aghighi M, Pisani L, Theruvath AJ, et al. Ferumoxytol Is Not Retained in Kidney Allografts in Patients Undergoing Acute Rejection. Mol Imaging Biol 2018;20(1):139-149.

182. Ku MC, Schreiber A, Delgado PR, et al. Fluorine ((19)F) MRI for Assessing Inflammatory Cells in the Kidney: Experimental Protocol. Methods Mol Biol 2021;2216:495-507.

183. Li XM, Yang L, Reng J, Xu GH, Zhou P. Non-invasive evaluation of renal structure and function of healthy individuals with multiparametric MRI: Effects of sex and age. Sci Rep 2019;9(1):10661.

184. de Boer A, Hoogduin JM, Blankestijn PJ, et al. 7 T renal MRI: challenges and promises. Magma (New York, NY) 2016;29(3):417-433.

185. Boehmert L, Kuehne A, Waiczies H, et al. Cardiorenal sodium MRI at 7.0 Tesla using a 4/4 channel (1) H/(23) Na radiofrequency antenna array. Magn Reson Med 2019;82(6):2343-2356.

186. Li X, Bolan PJ, Ugurbil K, Metzger GJ. Measuring renal tissue relaxation times at 7 T. NMR Biomed 2015;28(1):63-69.

187. Hoogduin H, Raaijmakers A, Visser F, Luijten P. Initial experience with BOLD imaging of the kidneys at 7 T. In: ISMRM, editor. Proceedings of the 22nd scientific meeting, ISMRM; 2014; Milan, Italy. ISMRM. (Proceedings of the 22nd scientific meeting, ISMRM).

188. Brinkmann I, Darji N, Speck O, Bock M. BOLD MRI of the Kidneys under water loading at 7 Tesla using parallel Transmission and RF Shimming of individual slices. Proc. Intl. Soc. Mag. Reson. Med. 22 2014; Milan, Italy. (Proc. Intl. Soc. Mag. Reson. Med. 22).

189. Li X, Auerbach EJ, Van de Moortele PF, Ugurbil K, Metzger GJ. Quantitative single breath-hold renal arterial spin labeling imaging at 7T. Magn Reson Med 2018;79(2):815-825.

190. Feng L, Axel L, Chandarana H, Block KT, Sodickson DK, Otazo R. XD-GRASP: Golden-angle radial MRI with reconstruction of extra motion-state dimensions using compressed sensing. Magn Reson Med 2016;75(2):775-788.

191. Feng L, Liu F, Soultanidis G, et al. Magnetization-prepared GRASP MRI for rapid 3D T1 mapping and fat/water-separated T1 mapping. Magn Reson Med 2021;86(1):97-114.

192. Kocanaogullari A, Ariyurek C, Afacan O, Kurugol S. Learning the Regularization in DCE-MR Image Reconstruction for Functional Imaging of Kidneys. IEEE Access 2022;10:4102-4111.

FIGURES:

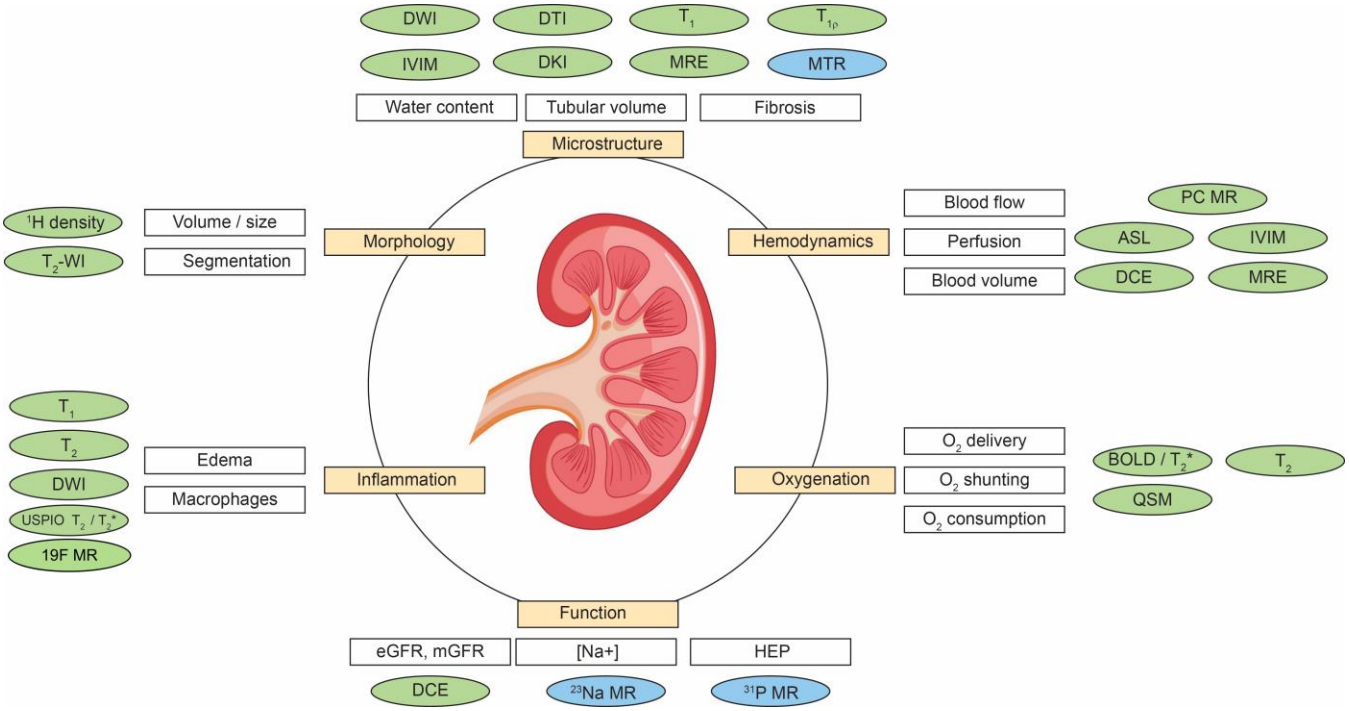

Figure 1: Diagram of renal functional markers from multiple approaches (nephrology, physiology, histopathology, quantitative MRI), with different but related connections to key features of renal health. Markers discussed in this review are shaded in green, and others not covered herein are shaded in blue. Continued efforts to flesh out these relationships, in both health and disease, will inform the development application of MRI as a surrogate or supplemental clinical marker. Abbreviations: ASL=arterial spin labelling; BOLD/T2*=blood oxygen level dependent; DCE=dynamic contrast-enhanced MRI; DWI=diffusion-weighted imaging; DKI=diffusion kurtosis imaging; DTI=diffusion tensor imaging; eGFR=estimated glomerular filtration rate; HEP=high energy phosphates; IVIM=intravoxel-incoherent motion model of diffusion; QSM=quantitative susceptibility mapping; MRE= MR elastography; MTR= magnetization transfer imaging; PC MR=phase-contrast MRI.

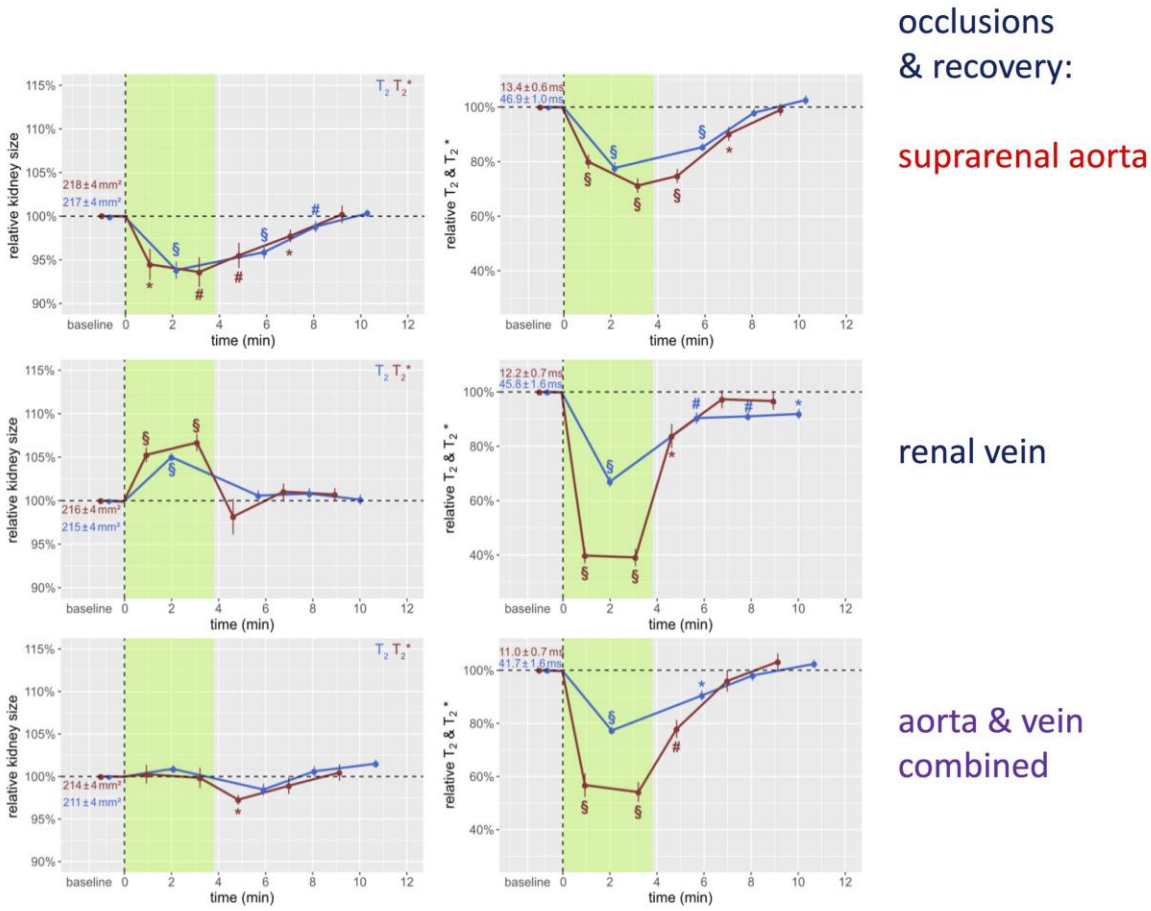

Figure 2: Time courses during kidney vascular occlusions and recovery. Time course of relative changes (mean±SEM) for kidney size (cross sectional area; left panels) and T_2 (blue) and T_2* (red) obtained for the renal cortex (right panels) before the occlusions (baseline), during the intervention (green area), and during recovery. Absolute baseline values (mean±SEM) are denoted; * $P < 0.05$; # $P < 0.01$; § $P < 0.001$. Data from Ref. 26 (Cantow et al., 2022).

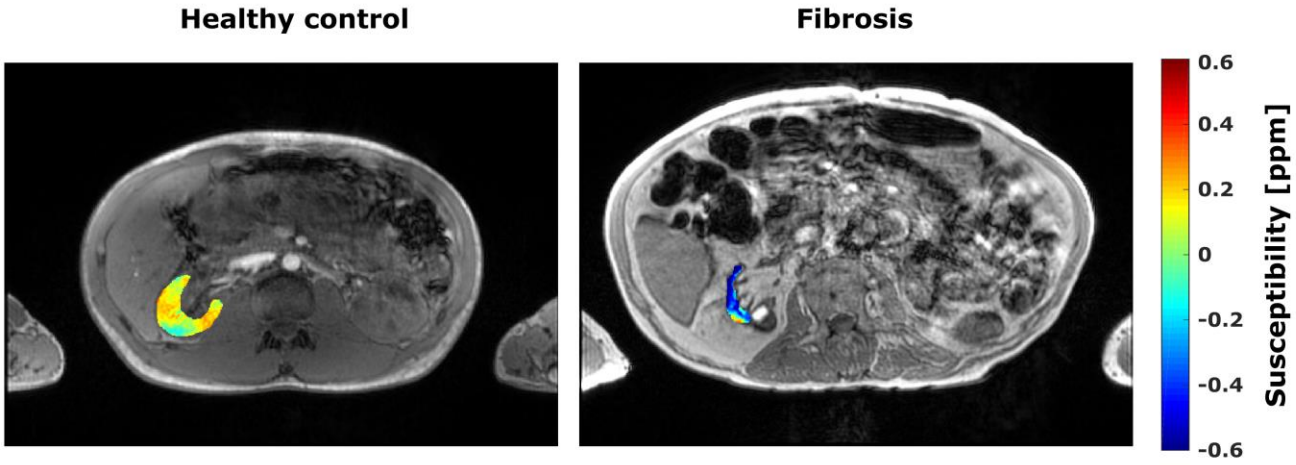

Figure 3: Magnitude images overlaid with QSM maps of the right kidney for a healthy volunteer (left image) and a patient with renal fibrosis (CKD V, eGFR < 15 ml/min/1.73 m^2, right image). Compared to the healthy renal tissue the fibrotic kidney shows a strong diamagnetic susceptibility (0.04 ± 0.07 ppm vs. -0.43 ± 0.02 ppm). Data from Ref. 80 (Bechler et al., 2021)

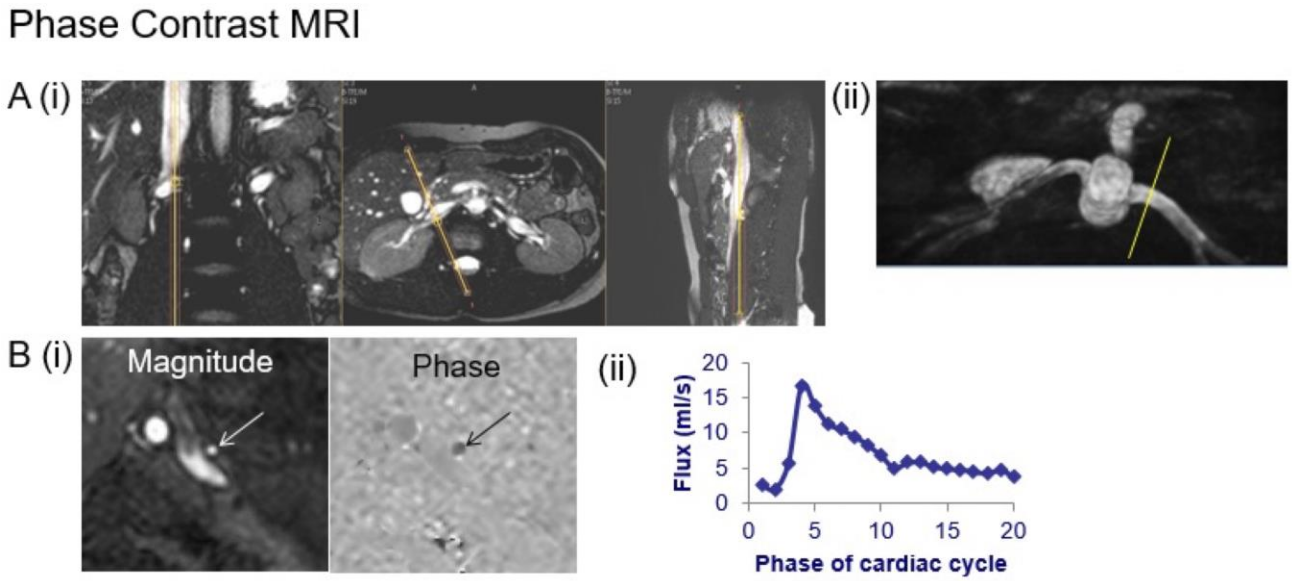

Figure 4: Phase contrast MRI is used to measure bulk flow within the renal artery. (A) The imaging plane must be perpendicular to the renal artery, planned using (i) orthogonal localisers or (ii) a vascular survey. (B) For each phase of the cardiac cycle, (i) magnitude and phase (proportional to velocity) images are acquired at each phase of the cardiac cycle, from which (ii) the arterial flux can be calculated.

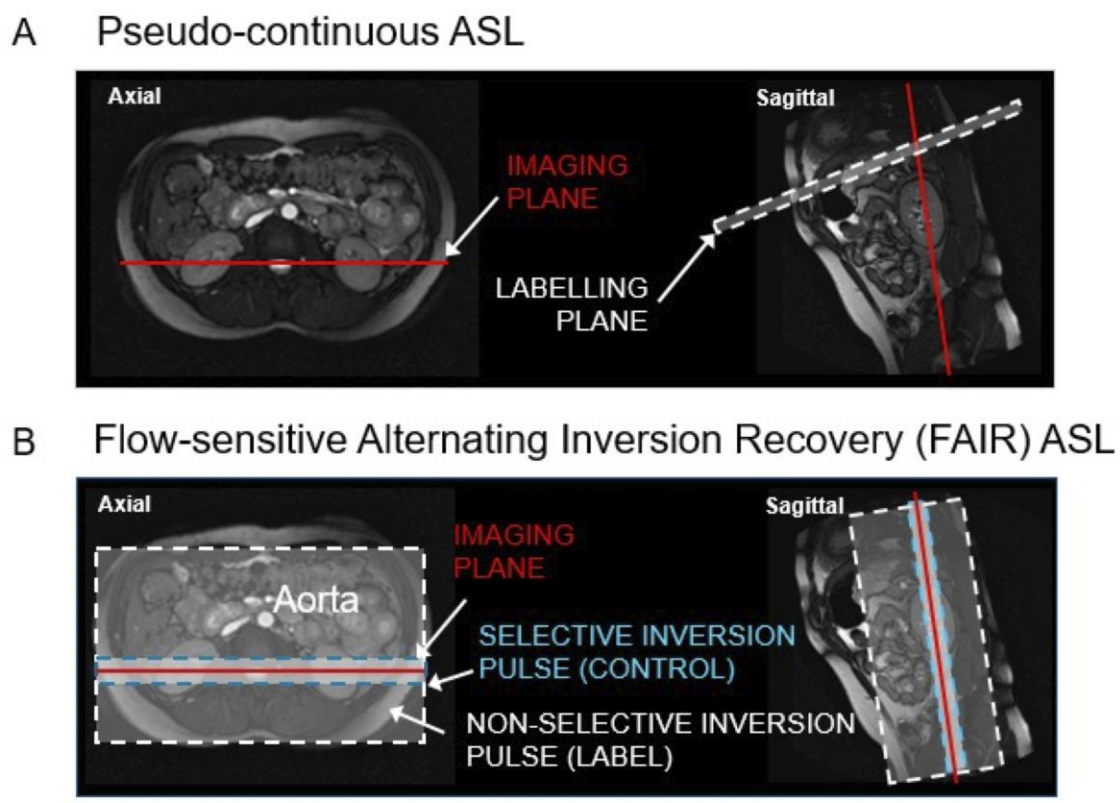

Figure 5: Schematic to illustrate planning of labeling and imaging planes for (A) pseudo-continuous arterial spin labeling (ASL) and (B) flow sensitive alternating inversion recovery (FAIR) ASL.

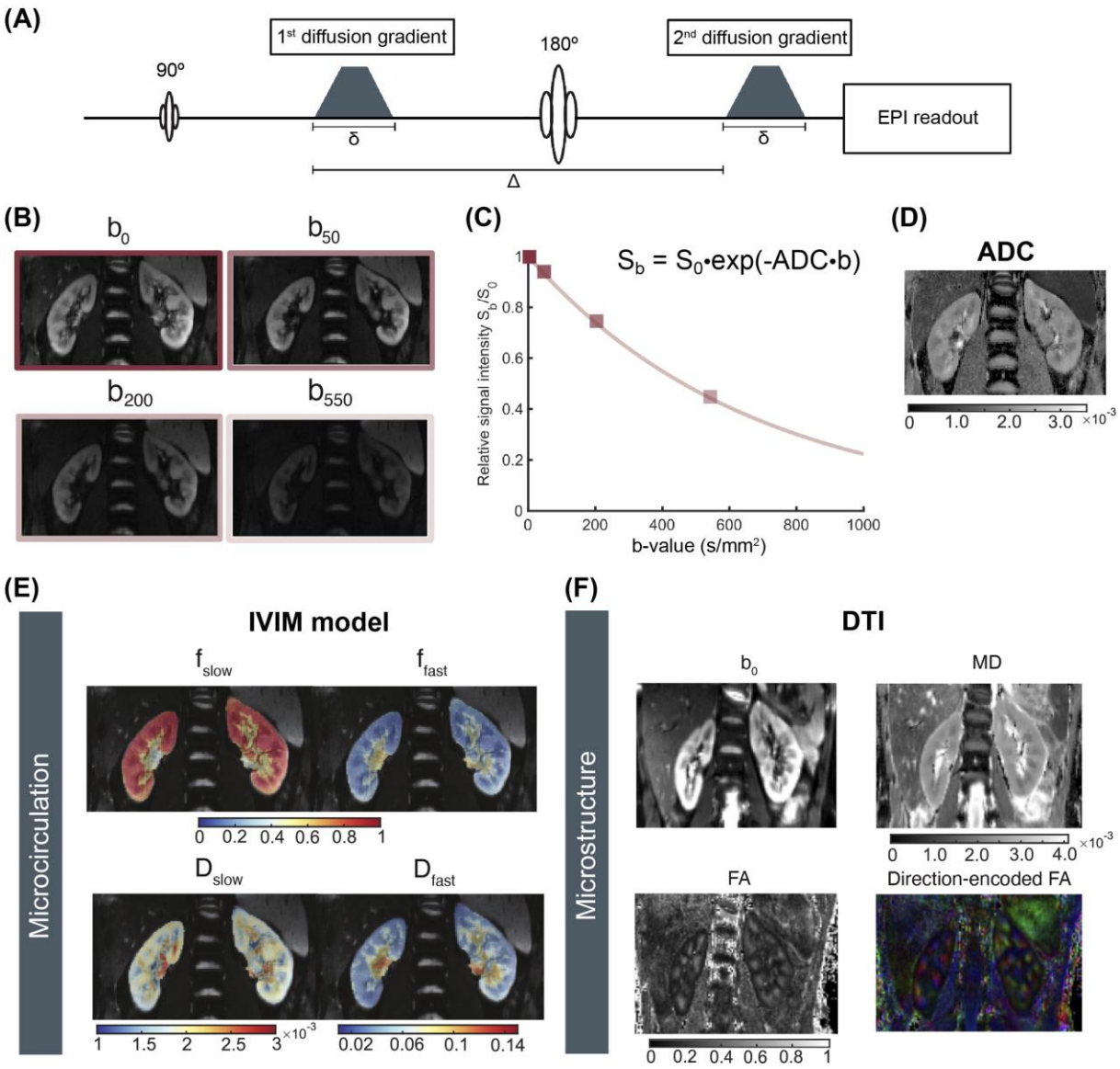

Figure 6: Renal microstructure and microcirculation measured by diffusion weighted imaging (DWI). (A) A schematic of the Stejskal-Tanner pulsed gradient spin echo experiment, which forms the basis of the current DWI pulse sequences; (B) DW images acquired at different b-values (with different levels of diffusion-weighting); (C) An ideal mono-exponential ADC fit to the noiseless DWI data; and (D) the corresponding ADC map. (E) Signal fractions (f_{slow} and f_{fast}) and (pseudo-) diffusion coefficient (D_{slow} and D_{fast}) parameter maps derived from DWI using intravoxel incoherent motion (IVIM) modelling. (F) Mean diffusivity (MD), fractional anisotropy (FA) and direction-encoded FA maps obtained from diffusion tensor imaging (DTI).

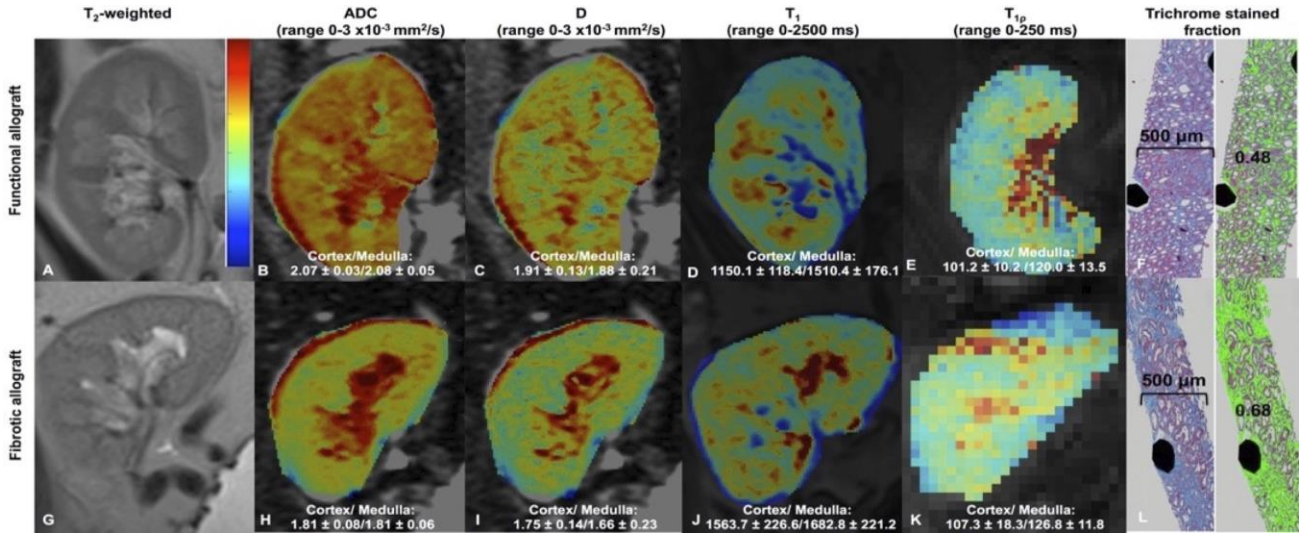

Figure 7. mpMRI in 55 year-old female patient with stable functional allograft (A-F; eGFR 78.4 ml/min/1.73m^2) and a 38 year-old female patient with dysfunctional allograft (G-L; eGFR 19.9 ml/min/1.73m^2) and fibrosis. ADC and D are decreased while T_1 and $T_1\rho$ are increased in both cortex and medulla in the fibrotic allograft.